Deep mutational scanning reveals tail anchor characteristics important for mitochondrial targeting

Abdurrahman Keskin[*†], Emel Akdoğan[*], Cory D. Dunn[*‡]

[*] Department of Molecular Biology and Genetics, Koç University, Sarıyer, İstanbul, Turkey

[†] Current affiliation:
Department of Biological Sciences
Columbia University
New York, NY 10027

[‡] Corresponding author
Dr. Cory Dunn
Koç Üniversitesi
Fen Fakultesi
Rumelifeneri Yolu
Sarıyer, İstanbul 34450
Turkey
Email: cdunn@ku.edu.tr
Phone: +90 212 338 1449
Fax: +90 212 338 1559

Running head: Comprehensive analysis of Fis1 TA

Abbreviations: TA, tail anchor; OM, outer membrane; MAD, membrane-anchoring domain; 3-AT, 3-aminotriazole; CHX, cycloheximide

ABSTRACT:

Proteins localized to mitochondria by a carboxyl-terminal tail anchor (TA) play roles in apoptosis, mitochondrial dynamics, and mitochondrial protein import. To reveal characteristics of TAs that are important for mitochondrial targeting, we examined the TA of the *Saccharomyces cerevisiae* Fis1 protein. We generated a library of Fis1p TA variants fused to the Gal4 transcription factor, then selected for mutations allowing Gal4 activity in the nucleus. Next-generation sequencing allowed quantification of TA variants in our mutant library both before and after selection for reduced TA targeting. High-throughput results were confirmed by further analysis of individual Fis1p TA mutants. Intriguingly, positively charged residues were more acceptable at several positions within the membrane-associated domain of the Fis1p TA than negatively charged residues. These findings provide strong, *in vivo* evidence that lysine and arginine can “snorkel,” stably associating with a lipid bilayer by placing their terminal charges at the membrane interface. Our work provides the first high-resolution analysis of an organelle targeting sequence by deep mutational scanning.

INTRODUCTION:

Proteins inserted within the mitochondrial outer membrane (OM) by a carboxyl-terminal tail anchor (TA) are important for programmed cell death, mitochondrial protein import, and the control of mitochondrial shape and number (Wattenberg and Lithgow, 2001). However, how proteins are targeted to mitochondria by TAs is not understood (Lee *et al.*, 2014; Neupert, 2015). TA targeting seems to depend upon incompletely defined structural characteristics of the TA rather than a defined consensus sequence (Beilharz, 2003; Rapaport, 2003; Borgese *et al.*, 2007). No components dedicated to TA insertion have been identified, and in fact, genetic and biochemical evidence suggest that spontaneous insertion of TAs might occur without the need for a translocation machinery (Setoguchi *et al.*, 2006; Kemper *et al.*, 2008). Such a mode of insertion stands in stark contrast with TA protein insertion into the endoplasmic reticulum (ER), which can take advantage of a conserved set of soluble proteins and membrane-bound receptors (Denic *et al.*, 2013; Johnson *et al.*, 2013).

Genetic selection schemes using the organism *Saccharomyces cerevisiae* have been of high value in understanding how proteins reach their proper destination within the eukaryotic cell. During such studies, a protein required for survival under selective conditions can be mislocalized, and thereby made inactive, by a targeting sequence utilized by the transport process being studied. Next, mutations that allow return of this mistargeted protein to a region of the cell at which it can perform its function are recovered under selective conditions. *Trans* factors related to protein targeting are identified by standard genetic approaches. Alternatively, *cis* mutations in the targeting sequence are revealed, typically by Sanger sequencing of individual fusion construct clones. Most prominently, this genetic approach to studying protein targeting and transport has been important in understanding protein transit to and through the endomembrane system (Deshaies and Schekman, 1987; Robinson *et al.*, 1988; Stirling *et al.*, 1992). This approach has also been applied to the study of protein import and

export at the mitochondrial inner membrane (Jensen *et al.*, 1992; Maarse *et al.*, 1992; He and Fox, 1999).

Even with the availability of powerful genetic strategies, a fine-grained analysis of any single eukaryotic protein targeting signal has been lacking. However, with the advent of next-generation sequencing, more comprehensive studies of protein targeting sequences are possible. In this study, we successfully coupled genetic selection to next-generation sequence analysis in order to reveal the structural and sequence characteristics important for localization of the tail-anchored Fis1 protein to the mitochondrial OM.

85 **RESULTS:**

86

87 *Localization to the mitochondrial outer membrane via the Fis1 tail anchor prevents*
88 *Gal4-mediated transcriptional activation*

89

90 The TA of Fis1p is necessary (Mozdy *et al.*, 2000; Beilharz, 2003) and sufficient
91 (Kemper *et al.*, 2008; Förtsch *et al.*, 2011) for insertion of this polypeptide into the
92 mitochondrial OM. Fis1p has been suggested to reach a final topology in the outer
93 membrane in which the amino-terminal bulk of the protein faces the cytosol, a very
94 short and positively charged carboxyl-terminus protrudes into the mitochondrial
95 intermembrane space, and the two are connected by a membrane-anchoring domain
96 (MAD) passing through the OM (Mozdy *et al.*, 2000). In developing our selection for TA
97 mutations that diminish Fis1p targeting, we reasoned that fusion of a transcription
98 factor to Fis1p would lead to insertion within the mitochondrial OM and a lack of
99 nuclear function (Figure 1A). Mutations within the TA of Fis1p that prevent effective
100 membrane insertion would, however, presumably allow the linked transcription factor
101 to enter the nucleus, promote expression of its targets, and allow survival under
102 specific selective conditions. Toward this goal, we fused the Gal4 transcription factor
103 to the amino-terminus of full-length Fis1p, since *S. cerevisiae* strains allowing titratable
104 selection based upon Gal4p potency are readily available. We included superfolder
105 GFP (Pédelacq *et al.*, 2005) between the Gal4 and Fis1 moieties, and upon
106 overexpression, GFP fluorescence was visible at mitochondria (Figure S1). Importantly,
107 the Gal4-Fis1p fusion failed to complement the mitochondrial morphology defect of a
108 *fis1Δ* mutant (Figure S1 and unpublished results), suggesting that our fusion protein
109 cannot interact effectively with other mitochondrial division components that might
110 potentially impede nuclear translocation of Gal4-Fis1p upon TA mutation.

111

112 To assess failed Gal4-Fis1p targeting to mitochondria, we specifically took advantage
113 of the Gal4-driven *HIS3* and *URA3* auxotrophic markers in MaV203, a strain commonly
114 used for yeast-two-hybrid assays (Vidal *et al.*, 1996a). Similar to cells containing an

115 empty vector, Gal4p fused to Fis1p was unable to provide growth on medium lacking
116 histidine and containing 20mM 3-aminotriazole (3-AT) to competitively inhibit any His3p
117 produced independently of Gal4p activation (Durfee *et al.*, 1993) or in medium lacking
118 uracil (SC-Ura) (Figure 1B). However, the same Gal4-Fis1 polypeptide devoid of its TA
119 [Gal4-Fis1(ΔTA)] provided ample proliferation on the same two selective media. This
120 result indicated that our fusion protein could translocate to the nucleus upon TA
121 disruption and that any potential lipid binding mediated by the cytosolic domain of
122 Fis1p (Wells and Hill, 2011) will not prevent genetic assessment of TA localization.
123
124 Following validation of our experimental approach, we immediately sought mutations in
125 the TA that would block targeting of Gal4-Fis1p to the mitochondrial OM by isolating
126 colonies spontaneously arising on medium lacking uracil. Limited sequencing of the
127 constructs encoding Gal4-Fis1p within these isolates revealed at least seven nonsense
128 and 19 frameshift mutations out of a total of 32 plasmids analyzed. While these
129 findings further validated the link between growth under selective conditions and
130 damage to the Fis1p TA, continued encounters with nonsense and frameshift
131 mutations would not be greatly informative regarding the sequential or structural
132 determinants important for TA targeting.
133
134 In the strain used for our selective scheme, a Ura^+ phenotype requires greater Gal4-
135 dependent transcriptional activation than a His^+ phenotype (Vidal *et al.*, 1996b).
136 Therefore, we reasoned that initial selection of TA mutants based on a His^+ phenotype
137 may provide informative mutations that weaken, but do not totally inhibit membrane
138 association. We used mutagenic PCR to generate altered TAs within the context of a
139 Gal4-Fis1 fusion protein. We then isolated four colonies that proliferated upon SMM-
140 His medium containing 20mM 3-AT, yet exhibited diminished proliferation on SC-Ura
141 medium when compared to cells expressing the Gal4-Fis1(ΔTA) polypeptide. Sanger
142 sequencing of the region encoding the TA of Gal4-Fis1p within these colonies revealed
143 one clone with a V145E mutation (amino acid numbering provided in this study will
144 correspond to that of the unmodified, full-length Fis1 protein), two clones with a L139P

145 mutation, and one clone with two mutations: L129P and V138A. Serial dilution assays
146 (Figure 2A) confirmed that V145E and L139P provided a less than maximal, but still
147 apparent Ura^+ phenotype, with the V145E mutant allowing more rapid proliferation on
148 medium lacking uracil than the L139P mutant. The L129P/V138A mutant provided a
149 His+ phenotype, but could not drive uracil prototrophy, suggesting a less severe
150 localization defect than that exhibited by the other two mutant TAs. Interestingly, the
151 V145E mutation falls within the MAD of the Fis1p TA, consistent with poor
152 accommodation of a charged amino acid within this hydrophobic stretch of amino
153 acids. Moreover, the Fis1p TA is predicted to be mostly alpha-helical in nature, so
154 isolation of the potentially helix-disrupting L139P replacement by selection may
155 indicate a need for TA helicity during mitochondrial targeting.
156
157 We then verified that these mutations presumably disrupting TA targeting are not
158 isolated merely as a consequence of the Gal4p-based selection system that we had
159 applied. Toward this goal, we took advantage of the Pdr1 transcription factor, which
160 promotes resistance to several drugs (Meyers *et al.*, 1992; Prasad and Goffeau, 2012).
161 The *PDR1-249* allele encodes a hyperactive Pdr1p that promotes cycloheximide (CHX)
162 resistance (Mutlu *et al.*, 2014). Fusion of the hyperactive Pdr1-249 protein to the
163 unmutated Fis1p TA did not allow CHX resistance (Figure S2). However, addition of the
164 V145E mutation to the TA in this fusion protein did permit CHX resistance, presumably
165 as Pdr1-249p entered the nucleus to activate its targets. These findings demonstrate
166 that mutations recovered using our Gal4p-based scheme are unlikely to be related to
167 the use of any specific transcription factor.
168
169 Transcription driven by Gal4-Fis1p indirectly reports on TA targeting to mitochondria
170 and may be affected by mutant stability, ability of the fusion protein to translocate to
171 the nucleus, or other events unrelated to normal TA localization. To further examine
172 whether isolated TA mutations affect mitochondrial OM targeting, we linked wild-type
173 (WT) or mutant Fis1p TAs to the carboxyl-terminus of mCherry. To assess
174 mitochondrial localization of these fusion proteins, mitochondria were specifically

175 labelled with GFP targeted to mitochondria by the presequence of the Cox4 protein
176 (Sesaki and Jensen, 1999). Importantly, the TA of Fis1p lacks information required for
177 mediating mitochondrial fragmentation (Habib *et al.*, 2003), indicating that the
178 localization of these constructs should not be influenced by interaction partners of full-
179 length, inserted Fis1p.
180
181 The location of mCherry fused to Fis1p TAs faithfully recapitulated our genetic findings.
182 V145E and L139P mutations in the Fis1p TA led to very substantial cytosolic
183 localization of mCherry (Figure 2B). Moreover, the L129P/V138A TA, consistent with its
184 weaker activation of Gal4 targets in our selection system, provided still discernable
185 mitochondrial localization of the mCherry signal, but cytosolic levels of this mutant
186 fusion protein appeared to be increased compared to mCherry fused to the WT TA.
187 These results suggest that, in general, our genetic approach is likely to accurately
188 report upon the ability of the Fis1p TA to moor proteins to the mitochondrial outer
189 membrane.
190
191 *Deep mutational scanning uncovers determinants of Fis1p tail-anchor targeting*
192
193 Buoyed by our initial isolation of TA mutations affecting mitochondrial localization, we
194 decided to take a more global approach to the analysis of the Fis1p TA. Using
195 degenerate primers and recombination-based cloning in *S. cerevisiae*, we sought to
196 generate a library consisting of all possible codons at every one of 27 amino acid
197 positions within the TA of Gal4-Fis1p. We then allowed the pool of cells containing
198 mutant TAs to divide four times under six possible culture conditions: no specific
199 selection for *HIS3* or *URA3* reporter activation (SC-Trp, selecting only for plasmid
200 maintenance), selection for *HIS3* activation at different 3-AT concentrations (SMM-Trp-
201 His +0, 5, 10, or 20mM 3-AT), or selection for *URA3* activation (SC-Ura). Plasmid DNA
202 was isolated from each pool of mutants, and TA coding sequences were amplified and
203 subjected to next-generation sequencing. We then focused our analysis only on those
204 clones within our pools that carried zero or one amino acid changes.

While all potential replacement mutations could not be detected within our starting library (Figure S3), and some biases did exist at each TA position, most potential amino acid mutations were represented within our pool. 98.9% of potential amino acid replacements were identified in the starting pool cultured in SC-Trp, and 95.9% of TAs with single mutations were represented by at least 10 counts. Quantification of counts from all samples can be found in Table S1. When comparing the mutant pool cultured in SC-Trp with selection in SMM-Trp-His without added 3-AT, there was no appreciable difference in the relative abundance of most mutant TAs, including truncation mutations expected to totally prevent mitochondrial targeting of Gal4-Fis1p (Figure S4A). Such a result is consistent with 'leaky' expression of *HIS3* independent of Gal4-driven activation (Durfee *et al.*, 1993). However, upon addition of 3-AT at concentrations of 5mM (Figure S4B), 10mM (Figure S4C), or 20mM (Figure 3) to medium lacking histidine, there were substantial shifts in the composition of the mutant pools toward specific amino acids, prompting further experiments that we describe below. The pool cultured in SC-Ura medium showed very strong selection for nonsense mutations within the TA (Figure S4D), but less prominent biases among amino acids. When considering our initial findings, in which recovery of uracil prototrophs by our genetic scheme led to a high recovery of frameshift and nonsense mutations, assessment of *HIS3* activation seems more informative regarding determinants of Fis1p TA targeting than competition assays performed in the more strongly selective medium lacking uracil.

Independently of the primary amino acid sequence, the specific codons used to direct synthesis of a protein can affect that polypeptide's translation rate and folding (Yu *et al.*, 2015). Although TAs shorter than the ribosome exit tunnel, which is 30 to 40 residues in length (Voss *et al.*, 2006), must certainly be inserted post-translationally, we also examined enrichment of specific codons following selection for Gal4-Fis1p presence in the nucleus. However, this approach did not provide notable evidence of a role for specific codons in directing localization of the Fis1p TA (Figure S5). While the data are more 'noisy' due to a lack of representation of certain codons at each

235 position, codons encoding the same amino acid generally acted in concert with one
236 another within our selection scheme, placing our focus on the amino acid sequence of
237 library variants rather than on codon sequence.
238
239 *Proline is not acceptable at many locations within the Fis1p tail anchor*
240
241 Previous analyses of tail-anchored mitochondrial proteins suggested that primary
242 sequence may not determine TA insertion (Beilharz, 2003; Rapaport, 2003; Borgese *et*
243 *al.*, 2007). Importantly, our global analysis demonstrates no apparent requirement for a
244 single, specific amino acid at any given position within the TA in order to achieve
245 membrane localization; most amino acid replacements within the WT TA sequence fail
246 to lead to selectable reporter activation (Figure 3). We focused our subsequent analysis
247 on general characteristics of the TA that might be important for mitochondrial OM
248 targeting.
249
250 The recovery of the L139P mutation during preliminary selection for Fis1p TA mutations
251 indicated that proline may not be acceptable within the hydrophobic core of the Fis1p
252 TA. Our deep mutational scan of the Fis1p TA in SMM-Trp-His+20mM 3-AT (Figure 3)
253 also strongly indicated that proline insertion across many positions disrupted
254 mitochondrial TA localization. When focusing specifically upon those mutants that were
255 in the top 75% most commonly counted variants in the starting pool (>126 counts) and
256 enriched at least four-fold in SMM-Trp-His + 20mM 3-AT, 12 of 33 missense mutations
257 within this set were proline replacements (Figure 4), further indicating failure of TA
258 targeting following placement of proline at many TA positions.
259
260 Subsequently, we carried out directed experiments to further examine poor
261 accommodation of proline within the Fis1p TA. We further studied the L139P mutant
262 that was initially isolated during selection for Fis1p TA targeting mutants, and we also
263 generated four additional, individual proline replacements within Gal4-Fis1p and tested
264 for Gal4-driven reporter activation. Newly constructed V134P, L139P, A140P, and

265 A144P substitutions, consistent with our larger scale analysis (Figure 3 or Figure 4),
266 provided ample proliferation on medium selective for *HIS3* activation (Figure 5A). We
267 noted that only the A144P substitution mutation provided strong proliferation on
268 medium lacking uracil (Figure S6A). Upon visualization of mCherry fused to these Fis1p
269 TA mutants, V134P, L139P, A140P, and A144P replacements all clearly diminished
270 mCherry localization to mitochondria (Figure 5B). Our results suggest that the
271 secondary structure of the Fis1p TA is important for its function, and that disruption of
272 helicity at many locations may make targeting to the mitochondrial OM unfavorable.
273
274 Curiously, the G137P mutation was not strongly enriched within the mutant pool during
275 selection (Figure 3). Consistent with these results, individual testing of this mutant
276 suggested poor activation of Gal4-dependent transcription (Figure 5A). Moreover,
277 mCherry fused to a Fis1p TA containing the G137P mutation remained strongly
278 localized to mitochondria (Figure 5B). Therefore, proline seems permissible at specific
279 positions within the MAD of the Fis1p TA.
280
281 For those mutant Fis1p TAs that cannot effectively direct mCherry to mitochondria, two
282 mechanisms may explain failure of mitochondrial localization. First, targeting to and
283 insertion at mitochondria may be impeded. Second, these mutant TAs may support
284 initial mitochondrial translocation, but a lack of stability within the lipid bilayer may lead
285 to ejection from the mitochondrial OM by a quality control mechanism. Recently, the
286 yeast Msp1 protein and its human ortholog ATAD1, have been identified as potential
287 'extractases' that can remove improperly folded or mislocalized proteins from the
288 mitochondrial OM (Chen *et al.*, 2014; Okreglak and Walter, 2014). We tested whether
289 any of tail-anchored fluorescent proteins containing proline replacements and not
290 strongly localized to mitochondria could recover mitochondrial localization in cells
291 deleted of Msp1p. However, deletion of Msp1p did not lead to relocalization of any
292 tested mutant mCherry-TA fusion protein to mitochondria (Figure 5C), providing no
293 evidence for proper targeting, then subsequent removal, of assayed Fis1p TAs
294 harboring proline replacements.

295 *Extension or reduction of Fis1p TA length does not affect targeting to mitochondria*
296
297 Targeting of tail-anchored proteins to specific membranes has been suggested to
298 depend, at least in part, upon the specific length of the MAD domain within the TA
299 (Isenmann *et al.*, 1998; Horie *et al.*, 2002). We reasoned that the region within the MAD
300 at which prolines do not strongly disrupt mitochondrial targeting may be amenable to
301 the insertion or deletion of new amino acids, thereby allowing us to test the relationship
302 between Fis1p TA length and mitochondrial targeting. We inserted one (∇1A), two
303 (∇2A), or three (∇3A) additional alanines between A135 and G136 within the TA of Gal4-
304 Fis1p, but none of these mutant constructs led to apparent *HIS3* (Figure 6A) or *URA3*
305 (Figure S6B) activation. We then analyzed the location of mCherry fused to a Fis1p TA
306 carrying these same insertions. All constructs were localized properly to mitochondria
307 (Figure 6B).
308
309 Next, we deleted one (ΔG136), two (ΔA135-G136), or three (ΔA135-G137) amino acids
310 within the Fis1p MAD and performed similar assays. Like our insertion mutants,
311 deletion mutants were apparently targeted to a membrane, as assessed by Gal4-driven
312 reporter transcription (Figure 6A and Figure S6B). Moreover, mCherry remained
313 localized to mitochondria when up to three amino acids were deleted (Figure 6C).
314
315 Disruption of the ER-localized Spf1 protein reduces the contrast in ergosterol content
316 between the ER and the mitochondrial OM (Krumpe *et al.*, 2012). Consequently, TAs
317 normally localized to mitochondria are mistargeted to the ER upon Spf1p deletion. The
318 sterol concentration of membranes can determine bilayer thickness (Dufourc, 2008),
319 raising the possibility that insertions or deletions may allow mitochondrial TAs to once
320 again prefer mitochondrial OM targeting over ER localization in the *spf1Δ* background.
321 However, mCherry linked to insertion or deletion mutants of the Fis1p TA remained
322 prominently localized to the ER in mutants lacking Spf1p (Figure S7).
323

324 Together, our results demonstrate that the Fis1p TA is targeted to mitochondria even
325 when its length is substantially altered.
326
327 *The hydrophilic carboxyl-terminus of the tail anchor allows specific targeting to*
328 *mitochondria*

329 Analysis of the data from our deep mutational scan suggested that nonsense
330 mutations throughout much of the TA can allow Gal4-Fis1p to move to the nucleus and
331 activate transcription (Figure 3, Figure 4, and Figure S4). Stop codons placed within the
332 highly charged RNKRR pentapeptide near the carboxyl-terminus of Fis1p, however,
333 seem to permit some membrane localization as reported by proliferation in selective
334 medium. Therefore, we examined the behavior of a R151X mutant, which lacks all
335 charged amino acids following the predicted MAD. Supporting partial localization to a
336 cellular membrane, the R151X mutant of Gal4-Fis1p did not activate Gal4-controlled
337 expression of *HIS3* to the same extent of a Gal4-Fis1p construct lacking the entire TA
338 (Figure 7A), nor did the R151X mutation lead to proliferation on medium lacking uracil
339 (Figure S6C). Consistent with those results, the R151X TA directed mCherry to
340 intracellular organelles (Figure 7B). However, along with some apparent mitochondrial
341 association, the R151X TA was also clearly localized to the ER. Interestingly, ER
342 localization of mCherry fused to the R151X TA occurred independently of Get3p, a
343 receptor for ER tail-anchored proteins (Schuldiner *et al.*, 2008), suggesting an
344 alternative, parallel pathway for localization of the R151X TA to the ER (Figure S8). Our
345 results demonstrate that the charged amino acids at the carboxyl-terminus of the TA
346 provide organelle specificity, yet are not totally required for membrane localization.
347 These findings are consistent with previous results reporting that positively charged
348 amino acids following the MAD of Fis1p allow mitochondrial targeting of TAs (Isenmann
349 *et al.*, 1998; Kuroda *et al.*, 1998; Borgese *et al.*, 2001; Stojanovski *et al.*, 2004), perhaps
350 by decreasing total TA hydrophobicity, a factor important for determining the final
351 location of a TA (Beilharz, 2003; Wattenberg *et al.*, 2007).

352

353 Since the R151X variant of Gal4-Fis1p activated Gal4-driven reporters, yet was at least
354 partially localized to the ER, we wondered if ER localization of any protein fused to
355 Gal4 might similarly lead to Gal4-driven transcription due to the physical continuity
356 between the ER and nuclear envelope. Therefore, we examined the TA of the human
357 FIS1 protein (hFIS1), since full-length hFIS1 can localize to ER in *S. cerevisiae*
358 (Stojanovski *et al.*, 2004). Indeed, we found that mCherry fused to the hFIS1 TA was
359 mostly localized to ER (Figure S9A). However, a fusion protein consisting of Gal4 fused
360 to the TA of hFIS1 did not provide *HIS3* activation (Figure S9B), indicating that the
361 hFIS1 TA is quantitatively membrane-targeted in *S. cerevisiae* and that activation of
362 Gal4-dependent reporters upon removal of the positively charged carboxyl-terminus
363 from Gal4-Fis1p is unlikely to be a consequence of ER localization.
364
365 Due to the mislocalization of the hFIS1 TA, we then investigated the possibility that
366 other mitochondrial TA proteins from human would be targeted improperly in *S.*
367 *cerevisiae*. We fused mCherry to the TA of human BAX, a region that is sufficient for
368 insertion at the mammalian mitochondrial OM (Schinzel *et al.*, 2004). While mCherry
369 signal was diminished in comparison with other mCherry fusion proteins examined in
370 this study and expressed under the same promoter, mCherry fused to the BAX TA was
371 properly targeted to mitochondria (Figure S9C). Gal4 fused to the BAX TA did not
372 activate selectable reporters (C. Dunn, unpublished results), suggesting effective
373 mitochondrial targeting mediated by the BAX TA.
374
375 *Positively charged amino acids are more acceptable than negatively charged amino*
376 *acids within the predicted transmembrane domain of the Fis1p tail anchor*
377
378 Our deep mutational scan of the Fis1p TA demonstrated that Gal4-Fis1p was generally
379 able to activate gene expression when aspartate or glutamate was placed within the
380 MAD (Figure 3). In fact, upon examination of those amino acid replacements found
381 within the top three quartiles of counts in the initial library and also enriched at least
382 four-fold upon culture in SMM-Trp-His + 20mM 3-AT, 18 of 33 missense mutations

383 were aspartate or glutamate substitutions (Figure 4). We were surprised to find that
384 placement of positively charged arginine or lysine residues appeared to be much more
385 acceptable within the MAD of Fis1p than aspartate or glutamate; none of the amino
386 acid substitutions within the high-count, high-enrichment set (Figure 4) derived under
387 selective conditions were by lysine or arginine.
388
389 To further pursue the possibility that positively charged amino acids can be
390 accommodated within the Fis1p MAD, we mutated four amino acids within the
391 hydrophobic stretch of the Fis1p TA to aspartate, glutamate, lysine, or arginine.
392 Specifically, we generated amino acid replacements at positions V132, A140, A144, or
393 F148, then retested these mutants under selection for Gal4-Fis1p transcriptional
394 activity. The results from our global analysis were verified, with aspartate and
395 glutamate mutations providing stronger reporter activation than lysine and arginine
396 mutations (Figure 8). Only the A144D mutation provided sufficient Gal4 activation for
397 proliferation on medium lacking uracil (Figure S6D), suggesting a very severe TA
398 localization defect caused by this TA mutation. We noted that these mutant Gal4-Fis1
399 constructs exhibit altered behavior at different temperatures. For example, lysine
400 substitutions clearly led to comparably elevated *HIS3* activity at 18°C at positions A140
401 and F148 (Figure S10A), and glutamate substitutions may provide moderately reduced
402 *HIS3* activity when compared to aspartate substitutions upon incubation at 37°C
403 (Figure S10B). This outcome is consistent with the idea that altered phospholipid
404 dynamics at different temperatures may lead to consequent changes to TA insertion
405 efficiency (de Mendoza and Cronan, 1983).
406
407 We then tested the ability of these charged Fis1p TAs to promote mitochondrial
408 localization of mCherry. At V132 and F148, positions within the MAD nearer to the
409 putative water-lipid bilayer interface, mutation to positively charged amino acids
410 allowed abundant localization to mitochondria (Figure 9A). In contrast, mutation to
411 negatively charged amino acids clearly hindered mitochondrial targeting. We noted that
412 F148D and F148E replacements hampered mitochondrial localization more severely

413 than V132D and V132E replacements. At position A144, lying more deeply within the
414 MAD, all charge mutations inhibited mCherry targeting to mitochondria to some
415 degree, but TAs containing A144D and A144E were less able to localize to
416 mitochondria than A144K or A144R. Finally, no mitochondrial localization was apparent
417 for any of the charge mutants tested at position A140. However, A140K and A140R
418 mutants differed from A140D and A140E mCherry-TA mutants by localizing to other
419 membranes within the cell, including the plasma membrane, rather than providing a
420 diffuse cytosolic signal. Taken together, our results demonstrate that positively
421 charged amino acids at several mitochondrial TA positions do not prohibit
422 mitochondrial targeting and are clearly more acceptable than negatively charged amino
423 acids at those same positions.
424
425 We then tested whether deletion of the OM extractase Msp1p might allow those
426 charged Fis1p TAs that poorly localize to mitochondria to recover their targeting to this
427 organelle. However, Msp1p removal did not permit relocalization of tail-anchored
428 fluorescent proteins to mitochondria (Figure 9B), supporting the idea that charge
429 replacements within the Fis1p TA lead to a failure of association with the OM rather
430 than enhanced removal from mitochondria.
431
432 We carried out assays to determine if Fis1p carrying charge mutations within their TAs
433 at V132, A144, or V148 can provide Fis1p activity. Negligible Fis1p activity at
434 mitochondria is apparently sufficient to promote mitochondrial fission (Habib *et al.*,
435 2003; Krumpe *et al.*, 2012), suggesting that even minimal localization and related
436 functionality at the OM would be detectable by functional assays. For example, when
437 Fis1p activity is absent, mitochondrial fission cannot proceed and unchecked fusion
438 leads to a unified mitochondrial network (Mozdy *et al.*, 2000). Interestingly, Fis1p
439 variants harboring charged residues, positive or negative, at positions V132, A144, or
440 V148 provided some Fis1p function when expressed from a plasmid in a *fis1Δ*
441 background, with the exception of the Fis1p carrying the A144D mutation, as indicated
442 by mitochondrial morphology (Figure 10A). To further investigate Fis1p activity,

443 mitochondrial morphology was further perturbed by treatment with sodium azide,
444 which leads to mitochondrial fragmentation in cells competent for mitochondrial
445 division (Fekkes *et al.*, 2000; Klecker *et al.*, 2015) and to facile visualization of
446 mitochondrial fission defects. Again, except for the A144D mutant, all Fis1p variants
447 tested were able to provide mitochondrial division activity (Figure 10B and Figure S11).
448
449 Next, we applied a genetic test of Fis1p function. When mitochondrial fusion is
450 blocked, unbalanced mitochondrial division leads to mitochondrial fragmentation
451 (Hermann *et al.*, 1998; Rapaport *et al.*, 1998) and consequent loss of mtDNA and the
452 ability to respire. If mitochondrial division is lacking, however, mtDNA is instead
453 maintained by cells unable to carry out mitochondrial fusion (Sesaki and Jensen, 1999;
454 Fekkes *et al.*, 2000; Mozdy *et al.*, 2000; Tieu and Nunnari, 2000). In a result consistent
455 with our microscopy-based analysis, we found that only the A144D variant of Fis1p
456 lacked activity and therefore allowed cells to maintain mtDNA when the mitochondrial
457 fusogen Fzo1p is removed (Figure 10C). All other variants provided sufficient fission
458 activity for mitochondrial fragmentation and consequent mtDNA loss in the absence of
459 Fzo1p. We note that upon selection for Gal4-driven reporter activation, only the A144D
460 charge mutant provided sufficient *URA3* activation for proliferation on medium lacking
461 uracil (Figure S6D), supporting the correspondence between each mutant TA's
462 targeting, as reported by Gal4-Fis1p transcriptional activity, and its functionality at the
463 mitochondrial surface. Taken together, our results demonstrate that positively charged
464 amino acids within the MAD can better promote Fis1p localization than negatively
465 charged amino acids, but that even negatively charged amino acids can be
466 accommodated within the MAD and lead to some low level of mitochondrial targeting.
467

468 **DISCUSSION:**

469

470 Using a deep mutational scanning approach, we explored structural characteristics of
471 the Fis1p TA important for targeting to the mitochondrial outer membrane. To our
472 knowledge, this work is the first application of this technique to the study of a
473 eukaryotic organelle targeting signal. Deep mutational scanning, when coupled to an
474 effective method of screening or selection, is very cost- and time-effective (Araya and
475 Fowler, 2011; Boucher *et al.*, 2014; Fowler and Fields, 2014). Mutant library generation,
476 subsequent pool selection, and next-generation sequencing were completed in just a
477 few months. Consequently, this approach generates far more useful data over a
478 shorter duration than, for example, alanine scanning mutagenesis or low-throughput
479 genetic selection followed by Sanger sequencing. Deep mutational scanning has
480 recently been applied successfully to other areas of study, such as membrane protein
481 insertion within bacteria (Elazar *et al.*, 2016), tumor suppressor structure and function
482 (Starita *et al.*, 2015), and the relationship between a polypeptide's evolutionary path
483 and its present fitness (Hietpas *et al.*, 2011; Melamed *et al.*, 2013).

484

485 *Positively charged amino acids within membrane inserted protein segments may*
486 *"snorkel" to the lipid bilayer surface*

487

488 Because there is a high energetic barrier to placing any charged residue into a lipid
489 bilayer (Cymer *et al.*, 2015), we were initially surprised to find that positively charged
490 amino acids within the MAD of the Fis1p TA promoted mitochondrial targeting far
491 better than negatively charged amino acids. However, it has been suggested that
492 lysine and arginine within a MAD can "snorkel," or integrate the uncharged portion of
493 their side chain into the hydrophobic milieu of the lipid bilayer and locate their positive
494 charges near polar head groups at the interface between the membrane and aqueous
495 environment (Segrest *et al.*, 1990; Monné *et al.*, 1998; Strandberg and Killian, 2003;
496 Schow *et al.*, 2010). Some phospholipid head groups carry a net negative charge,
497 potentially providing further favorability to snorkeling lysine and arginine. The shorter

498 hydrophobic portion of aspartate and glutamate, however, may not permit the side
499 chain to easily reach the membrane interface in order to remove the negative charge
500 from the hydrophobic environment, and if they do reach the lipid bilayer surface,
501 charge repulsion might make such a conformation unfavorable. Snorkeling has been
502 visualized, for instance, during structural studies of the Kv1.2 potassium channel (Long
503 *et al.*, 2005) and integrin β3 (Kim *et al.*, 2012). However, little *in vivo* or functional
504 evidence has been reported supporting the snorkeling of amino acids located within
505 MADs. Our deep mutational scan of the Fis1p TA, a region dedicated only to the
506 process of mitochondrial OM integration (Habib *et al.*, 2003; Kemper *et al.*, 2008),
507 strongly suggests the ability of lysine or arginine to be accommodated by snorkeling at
508 numerous positions within the Fis1p MAD. We note that snorkeling, if operative for
509 positive charges within the Fis1p TA, may not be permitted within the context of all
510 mitochondrial TAs: replacement of S184 within the BAX TA by lysine does not seem to
511 permit mitochondrial localization of this protein (Nechushtan *et al.*, 1999).
512
513 Further deep mutational scans of MADs may further support the concept of snorkeling.
514 Interestingly, since those Fis1p TAs mutated to contain positively charged amino acids
515 within the MAD were not targeted to the OM with full efficiency, one might imagine a
516 scenario in which proteins evolve positively charged amino acid substitutions within
517 MADs previously lacking such charges so that dual localization to cytosol and to
518 intracellular membranes can be simply achieved. Certainly, current prediction methods
519 for MADs might be considered overly conservative, and further evidence of snorkeling
520 should prompt the development of improved algorithms that consider positively
521 charged amino acids to be acceptable within certain positions of a predicted MAD.
522
523 *The membrane-associated domain of the Fis1p tail-anchor may consist of two*
524 *separable segments*
525
526 Computational analyses suggest that the Fis1p TA is mostly alpha-helical in nature
527 (Buchan *et al.*, 2013; Drozdetskiy *et al.*, 2015). We found that proper localization of the

528 Fis1p TA likely requires its predicted alpha-helicity within the MAD, since proline, which
529 is known to break or kink helices (Senes *et al.*, 2004), profoundly disrupts targeting
530 when substituted at many positions throughout this hydrophobic region. However, we
531 found that replacement by proline is more acceptable at a specific location, G137, than
532 proline mutations found at previous or subsequent locations within this region,
533 potentially indicating that the Fis1p MAD is bipartite in nature. Further supporting a
534 bipartite structure of the Fis1p MAD, insertion of new amino acids between A135 and
535 G136 did not apparently affect mitochondrial TA targeting. Moreover, mutations toward
536 the carboxyl-terminal end of the Fis1p MAD appear to affect mitochondrial targeting
537 more drastically, as reported by deep mutational scanning, than mutations toward the
538 amino terminus of the transmembrane segment. Previous analysis of the yeast Tom5p
539 TA and rat OMP25 TA also support a bipartite structure of the MAD, with higher
540 sensitivity to mutation nearer to the carboxyl-terminal end of this hydrophobic stretch
541 (Horie *et al.*, 2002). In addition, prolines are found within the MAD of the mammalian
542 OMb and OMP25 TAs, and a proline within the MAD of Tom5p has been demonstrated
543 to be important for targeting to mitochondria (Allen *et al.*, 2002). These results suggest
544 that those prolines might demarcate the boundary between distinct structural regions
545 of the targeting sequence. On the other hand, prolines within a single helical segment
546 may simply be more easily housed within an alpha-helix when buried deep in the lipid
547 bilayer (Li *et al.*, 1996; Senes *et al.*, 2004) and may not reflect two separable MAD
548 segments. If this is the case, prolines found in mitochondrial TAs might indicate the
549 portion of the TA found at the midpoint of the OM.

550 Glycine is not preferred within alpha-helices (Chou and Fasman, 1974; O'Neil and
551 DeGrado, 1990) as a consequence of its conformational flexibility. However, our deep
552 mutational scan does not indicate reduced membrane targeting when most amino
553 acids within the Fis1p TA are individually mutated to glycine. This might be surprising
554 in light of the pronounced effects provided by several proline replacement mutations
555 throughout this domain. However, glycine may not be as disruptive for alpha-helices
556 found within a lipid bilayer environment when compared with alpha-helices of soluble

557 proteins, due to better intra-helical hydrogen bonding within the hydrophobic
558 environment of the membrane (Dong *et al.*, 2012). Indeed, four glycines already exist
559 within the *S. cerevisiae* Fis1p TA. The TAs of Fis1p orthologs are also littered with
560 glycines (Stojanovski *et al.*, 2004), further indicating that glycines are less disruptive of
561 the Fis1p TA than prolines. Interestingly, GXXXG motifs, and other similarly spaced
562 small amino acids like alanine and serine, can promote helix packing within lipid
563 bilayers (Russ and Engelman, 2000; Gimpelev *et al.*, 2004; Senes *et al.*, 2004).
564 However, our findings demonstrate that the sole Fis1p GXXXG motif and a nearby
565 AXXXA motif do not play a significant role in targeting of the Fis1p TA to membrane.
566
567 *The Fis1p tail anchor may not be exposed to the intermembrane space*
568
569 Four of five carboxyl-terminal residues of Fis1p are positively charged. Previous reports
570 indicated that a positively charged carboxyl-terminus is important specifically for
571 proper Fis1p targeting and generally for insertion of several other TAs at the
572 mitochondrial OM (Isenmann *et al.*, 1998; Horie *et al.*, 2002; Habib *et al.*, 2003; Horie *et*
573 *al.*, 2003; Yoon *et al.*, 2003; Stojanovski *et al.*, 2004). Further supporting the importance
574 of this highly charged region, our genetic selection and subsequent microscopic
575 analysis revealed that the last five amino acids within the Fis1p sequence are important
576 for effective insertion, as indicated by our genetic assessment, and for membrane
577 specificity, as indicated by our microscopic analysis. How this charged region
578 promotes localization and insertion is not yet clear.
579
580 The currently accepted view of Fis1p topology is that this positively charged carboxyl-
581 terminus is ultimately exposed to the mitochondrial intermembrane space. However, a
582 presumably high energetic barrier (Parsegian, 1969; Engelman and Steitz, 1981; Honig
583 and Hubbell, 1984) makes it difficult to countenance the transfer of the highly charged
584 carboxyl-terminus of mitochondrial TA proteins across a lipid bilayer without the
585 assistance of an aqueous pore. Interestingly, organellar import of mitochondrial TA-
586 containing proteins appears saturable in mammalian cells (Setoguchi *et al.*, 2006),

587 potentially indicating a finite number of translocons capable of transporting
588 mitochondrial TAs. Furthermore, the TOM complex has been reported to assist in
589 insertion of full-length BAX into mitochondria (Ott *et al.*, 2007; Cartron *et al.*, 2008;
590 Colin *et al.*, 2009). Potentially consistent with the need for a mitochondrial TA
591 translocation machinery, the hFIS1 TA localizes specifically to mitochondria in human
592 cells (Suzuki *et al.*, 2003), but cannot effectively localize mCherry to *S. cerevisiae*
593 mitochondria, possibly suggesting evolutionary divergence and a structural mismatch
594 between the hFIS1 TA and the putative yeast TA translocation apparatus. However, we
595 note that not all human mitochondrial TAs fail to be imported at the proper organelle in
596 yeast, since our genetic and microscopic results indicate that the human BAX TA is
597 properly inserted into yeast mitochondria.
598
599 Other evidence supports the idea that mitochondrial tail-anchored proteins like Fis1p
600 do not require a translocation machinery and can spontaneously insert into the OM.
601 First, the MAD of the TA is protected from chemical modification upon exposure to
602 lipid vesicles devoid of protein (Kemper *et al.*, 2008), suggesting that the Fis1p TA can
603 insert into lipid bilayers without assistance. Moreover, blockade or destruction of the
604 general insertion pore for mitochondrial proteins, associated receptors, or other outer
605 membrane protein biogenesis machinery such as the SAM complex or the MIM
606 complex did not prevent Fis1p insertion at yeast mitochondria (Stojanovski *et al.*, 2007;
607 Kemper *et al.*, 2008; Sinzel *et al.*, 2016). Tail-anchored proteins also appear to have the
608 ability to spontaneously and rapidly insert into mammalian mitochondria without the
609 need for the TOM complex or soluble cytosolic chaperones (Setoguchi *et al.*, 2006),
610 although cytosolic factors likely play a role in maintaining solubility stability of tail-
611 anchored proteins while they are *en route* to mitochondria (Itakura *et al.*, 2016). Further
612 supporting the absence of a translocation machinery dedicated to TA insertion, a large-
613 scale screen for proteins required for proper localization of mitochondrial tail-anchored
614 proteins uncovered no putative translocon components (Krumpe *et al.*, 2012). Finally,
615 although not evaluated in this work due to strong repression of peroxisome biogenesis
616 under the culture conditions utilized (Einerhand *et al.*, 1991; Van der Leij *et al.*, 1993), a

617 small fraction of cellular Fis1p may function at peroxisomes to mediate peroxisomal
618 fission (Koch *et al.*, 2005; Kuravi *et al.*, 2006). A machinery that allows Fis1p TA
619 insertion would potentially be shared by both mitochondria and peroxisomes, but no
620 dual-localized translocation machinery has yet been identified.
621
622 How can one reconcile abundant evidence for spontaneous insertion of TAs into the
623 mitochondrial OM with the presence of a highly charged region at the carboxyl-
624 terminus of the Fis1p TA that has been assumed to be translocated? We suggest the
625 possibility that while the Fis1p TA is inserted into the mitochondrial OM, it does not
626 reach through to the intermembrane space. Rather, the Fis1p TA may be mostly buried
627 within the outer leaflet of the OM, making transit of the positively charged terminus
628 through the lipid bilayer unnecessary. Such a scenario is supported by studies
629 suggesting that the TA of BAX is constantly inserted into the mitochondrial OM in non-
630 apoptotic cells, then removed from the mitochondrial surface and returned to the
631 cytosol (Edlich *et al.*, 2011; Schellenberg *et al.*, 2013). Constitutive extraction of BAX
632 that has completely passed through the OM and exposes polypeptide to the
633 intermembrane space seems unnecessarily expensive from an energetic standpoint.
634 Rather, it is conceivable that the TA of inactive BAX is monotopically integrated within
635 the plane of the membrane, thereby facilitating recycling. If true, Fis1p may take on a
636 similar topology due to structural similarity between the BAX and Fis1p TAs. Moreover,
637 the snorkeling of lysine or arginine placed into the Fis1p TA that is suggested by
638 findings reported here is consistent with both bitopic and monotopic insertion
639 (Strandberg and Killian, 2003). A caveat regarding any model in which Fis1p is
640 monotopic at the OM is that neither the WT Fis1p TA nor any functional TA charge
641 mutants produced in this study are characterized by the predicted amphiphilicity that is
642 thought to promote oblique insertion at membranes (Sapay *et al.*, 2006). We would like
643 to note that some form of membrane insertion is likely important for Fis1p functionality;
644 our preliminary studies suggest that replacement of the TA in Fis1p with a domain from
645 the Num1 protein that promotes peripheral association with the mitochondrial outer

membrane (Ping *et al.*, 2016) did not allow for mitochondrial division (A. Keskin, unpublished results).

Computational modeling informed by our high-throughput dataset, as well as further experimental work, will allow testing of whether Fis1p is monotopic or truly passes through the mitochondrial OM. Moreover, if a TA insertion machinery does exist at the mitochondrial OM, loss-of-function mutations affecting this machinery would presumably be recovered by the application of our genetic selection scheme. Finally, refined analysis of other organelle targeting signals and membrane insertion sequences can be accomplished by applying the deep mutational scanning approach outlined in this study.

657 **MATERIALS AND METHODS:**

658

659 *Yeast strains and plasmids*

660

661 Details of strains used in this study are provided in Table S2. Plasmid acquisition
662 details and associated references, as well as details of plasmid construction, are found
663 in Table S3. Oligonucleotides used in this study are listed in Table S4.

664

665 *Culture conditions*

666

667 Synthetic complete (SC) medium contains 0.67% yeast nitrogen base without amino
668 acids, 2% dextrose, 0.1% casamino acids, 50 µg/ml adenine hemisulfate, and either
669 25 µg/ml uracil (SC-Trp) or 100 µg/ml L-tryptophan (SC-Ura). Supplemented minimal
670 medium (SMM) contains 0.67% yeast nitrogen base without amino acids, 2% dextrose,
671 20 µg/ml adenine hemisulfate, 20 µg/ml uracil, 20µg/ml methionine, 30 µg/ml lysine.
672 SMM also contains, depending on selection needs, 20 µg/ml histidine, 100 µg/ml
673 leucine, and/or 20 µg/ml tryptophan, as indicated. SLac medium lacking histidine
674 contains 0.67% yeast nitrogen base without amino acids, 1.2% NaOH, a volume of
675 lactic acid sufficient to subsequently bring the pH to 5.5, 20 µg/ml adenine hemisulfate,
676 20 µg/ml uracil, 20 µg/ml methionine, 30 µg/ml lysine, 100 µg/ml leucine, and 20 µg/ml
677 tryptophan. Solid media also contain 1.7% bacteriological agar. Cells were incubated
678 at 30˚C unless otherwise indicated. For serial dilution assays, strains in logarithmic
679 proliferation phase were diluted to an OD_{600} of 0.1, and 4 µL of this dilution and three
680 serial five-fold dilutions were spotted to solid medium.

681

682 *Assessment of Fis1p function using a mtDNA loss assay*

683

684 Cells lose mtDNA and the ability to proliferate on non-fermentable medium when
685 mitochondrial fusion is blocked unless mitochondria division is also abrogated (Sesaki
686 and Jensen, 1999; Fekkes *et al.*, 2000; Mozdy *et al.*, 2000; Tieu and Nunnari, 2000).

687 Strain CDD688 (Mutlu *et al.*, 2014) harbors chromosomal deletions in *FZO1* and *FIS1*
688 and a CHX-counterselectable plasmid expressing *FZO1*. Upon removal of plasmid-
689 expressed *FZO1*, cells will maintain mtDNA and respire unless functional *FIS1* allowing
690 mitochondrial division is also present. To assess the functionality of Fis1p variants
691 containing TA mutations, strain CDD688 was transformed with plasmids expressing
692 WT *FIS1* or variants mutated within the Fis1p TA. Transformants were cultured
693 overnight in SMM-His medium lacking CHX to permit cells to lose the *FZO1*-encoding
694 plasmid. Serial dilutions were then spotted to SLac-His+3 µg/mL CHX ("lactate / no
695 fusion") and incubated for 5 d to test for maintenance of mtDNA following
696 counterselection for *FZO1*, with cell proliferation indicating a lack of Fis1p function. As
697 a control for cell proliferation under conditions not selective for mtDNA maintenance,
698 an equal number of cells was also spotted to SMM-Trp-His medium ("glucose /
699 fusion") and incubated for 2 d.
700
701 *Microscopy*
702
703 For epifluorescence microscopy, cells in the logarithmic phase of proliferation were
704 examined using an Eclipse 80i microscope with a 100X Plan Fluor objective and linked
705 to a DS-Qi1Mc camera (Nikon, Tokyo, Japan). Cells were cultured in SMM medium
706 appropriate for plasmid selection. Exposure times were automatically determined, and
707 images were captured using NIS-Elements version AR 3.2. All images of mCherry
708 expression were brightness adjusted in Adobe Photoshop CS5 (Adobe, San Jose,
709 California) to an equivalent extent, except when the mCherry-BAX(TA) signal was
710 assessed. For presentation of data associated with this fusion protein, the 'autolevels'
711 adjustment was used. Scoring of mitochondrial morphology was performed blind to
712 genotype. To promote mitochondrial fragmentation, sodium azide was added at a
713 concentration of 500 µM for 60 min before fluorescence microscopy. For staining of
714 mitochondrial nucleoids, 4'6-diamidino-2-phenylindole (DAPI) was added to cultures at
715 a concentration of 1 µg/ml and cells were incubated for 15 min before analysis.
716

717 *Fis1p TA mutant library construction*

718

719 Recombination-based cloning (Oldenburg *et al.*, 1997) was used to generate
720 constructs expressing Gal4-Fis1p and mutated at one of 27 positions within the Fis1p
721 TA. Two DNA segments generated by PCR were fused in this recombination reaction.
722 The 5' portion was amplified by PCR from template plasmid b100 using primer 698 and
723 the appropriate primer (rvsposX) listed in Table S4. The 3' section was generated from
724 template b100 using primers 517 and the relevant primer (fwdposX) listed in Table S4.
725 PCR products were recombined into *Not*I-linearized pKS1 by co-transformation of
726 vector and PCR products into strain MaV203. Each sub-library for each Fis1p TA
727 position was generated individually by selection of Trp^+ clones in liquid medium, with a
728 portion of each transformation reaction plated to solid SC-Trp medium to confirm
729 recombination and transformation efficiency. To generate the total pool prior to
730 selection for Gal4p-mediated transcription, equal numbers of cells, as determined by
731 OD_{600} measurement, were taken from overnight cultures of each sub-library and
732 combined within the same liquid culture. Note that all constructs expressing Gal4-
733 Fis1p also contain superfolder GFP (Pédelacq *et al.*, 2005)(REF) in frame between the
734 Gal4p and Fis1p segments, but for simplicity, this is typically omitted from figure labels
735 and from the text.

736

737

738 *Deep mutational scanning of the Fis1p TA library*

739

740 The pool of constructs containing Fis1p TA mutations was cultured for four generations
741 in SC-Trp medium, SC-Ura medium, or SMM-Trp-His medium containing 0 mM, 5 mM,
742 10 mM, or 20 mM 3-AT. Plasmids present under each culture condition were then
743 harvested from 10 OD_{600} units of cells. To harvest each plasmid library, cells were
744 pelleted at 4,000g for 3 min, then washed with 5 ml 0.9 M D-sorbitol and resuspended
745 in 1 ml of 0.9 M D-sorbitol. One "stick-full" of zymolyase 20T (Amsbio, Abingdon,
746 United Kingdom), was added, and cells were incubated at 37°C for 45 min. Cells were
747 again collected at 4,000g for 3 min and processed using a plasmid purification kit
748 (GeneJET Plasmid Miniprep Kit, Thermo Scientific, Waltham, USA) using the
749 manufacturer's instructions. Primers 882 and 883 were used to amplify the genomic
750 region encoding the Fis1p TA from each plasmid pool. Using the provided PCR
751 products, next-generation, paired-end sequencing was performed by Microsynth
752 (Balgach, Switzerland) on a MiSeq Nano (2x150v2). The resulting FASTQ output can be
753 found at [to be uploaded to Dryad Digital Repository and link provided, article
754 acceptance required for upload]. FASTQ output from paired ends and lacking adaptor
755 sequences was combined into a single segment using the PANDAseq assembler
756 version 2.8 (Masella *et al.*, 2012). The TRIM function (trimmer Galaxy tool version 0.0.1)
757 was performed using the resources of the Galaxy Project (Goecks *et al.*, 2010) in order
758 to remove sequences not directly encoding the defined Fis1p and stop codon. Further
759 processing in Microsoft Excel (Redmond, USA) subsequently allowed conversion of
760 DNA sequence to amino acid sequence and removal of those TAs with more than one
761 amino acid mutation from further analysis. Enrichment values reflect, at a given amino
762 acid position, the ratio of the fraction of amino acid counts following selection to the
763 fraction of amino acid counts in the starting library. Enrichment values are not derived
764 through comparisons across different amino acid positions. Counts for the native
765 amino acid at each position were set as the total number of TA counts for which all
766 amino acids were WT within a given selected pool. When calculating enrichment
767 values, TA amino acid replacements for which there were zero reads in the SC-Trp

768 sample had their value changed to one in order to allow possible detection of
769 enrichment under selective conditions by preventing division by zero. Heat maps were
770 generated using the Matrix2png utility (Pavlidis and Noble, 2003).

ACKNOWLEDGEMENTS:

We thank Gülayşe İnce Dunn, Bengisu Seferoğlu, Güleycan Bal, Funda Kar, and Sara Nafisi for comments on this manuscript. This work was supported by a European Research Council Starting Grant (637649-RevMito) to CDD, by a European Molecular Biology Organization Installation Grant (2138) to CDD, and by Koç University.

CONFLICT OF INTEREST STATEMENT:

The authors have no known conflict of interest affecting the outcome or interpretation of this study.

783 **FIGURE LEGENDS:**

784

785 **Figure 1.** A genetic selection based on protein mislocalization allows recovery of
786 mutations blocking Fis1p TA localization to mitochondria. (A) A scheme for selection of
787 mutations preventing mitochondrial targeting of the Fis1p TA. Full-length Fis1p is fused
788 to the transcription factor Gal4p (and to superfolder GFP, not shown). Upon failure to
789 localize Fis1p at the mitochondrial OM, Gal4p is free to translocate to the nucleus and
790 activate *HIS3* and *URA3*. (B) Removal of the Fis1p TA allows proliferation on medium
791 requiring *HIS3* activation or *URA3* activation. Strain MaV203 expressing Gal4-Fis1p
792 variants from plasmids b100 (WT), b101 (ΔTA), or harboring empty vector pKS1 was
793 cultured in SC-Trp medium, then, following serial dilution, spotted to SC-Trp, SMM-His
794 + 20 mM 3-AT, or SC-Ura and incubated for 2 d.

795

796 **Figure 2.** Selection for reporter activation by Gal4-Fis1p reveals TA mutations required
797 for full mitochondrial localization. (A) Missense mutations within the Fis1p TA provide
798 selectable marker activation. Strain MaV203 expressing Gal4-Fis1p variants from
799 plasmids b100 (WT), b128 (V145E), b129 (L139P), b130 (L129P, V138A), or b101 (ΔTA)
800 were treated as in Figure 1B. (B) Missense mutations within the Fis1p TA allow
801 cytosolic accumulation of a linked mCherry protein. mCherry fused to variants of the
802 Fis1p TA were expressed in WT strain CDD961 from plasmids b109 (WT), b134
803 (V145E), b135 (L139P), b136 (L129P,V138A), or b252 (ΔTA) and visualized by
804 fluorescence microscopy. Mitochondria were labelled with a mitochondria-targeted
805 GFP expressed from plasmid pHS1. Scale bar, 5 μm.

806

807 **Figure 3.** Mutations within the TA of a Gal4-Fis1 fusion protein allow Gal4-driven
808 transcription. The $\log_2$ of enrichment values for each amino acid were calculated for
809 each position following selection in SMM-Trp-His medium containing 20 mM 3-AT.
810 Enrichment values are generated for individual amino acid positions within the TA, and
811 not across positions. Black outlines denote the native amino acid for each position.

812 Amino acid replacements not detectable under selective conditions are denoted by
813 black, filled squares. The predicted MAD is indicated by a red line.
814
815 **Figure 4.** Identification of abundant Gal4-Fis1p clones which are highly enriched upon
816 selection for Gal4-Fis1p nuclear translocation. (A) TA replacement mutations are
817 plotted, with $\log_2$ enrichment values provided on the X-axis and sequence counts
818 recovered from the starting pool (SC-Trp) provided on the Y-axis. Those replacement
819 mutations that are within the top 75th percentile of mutant abundance in the starting
820 pool and enriched at least four-fold following selection in SMM-Trp-His medium
821 containing 20 mM 3-AT are highlighted in a blue box. (B) Expansion of the highlighted
822 region in (A) showing specific TA mutations.
823
824 **Figure 5.** Proline substitution is acceptable at a discrete position within the Fis1p TA.
825 (A) Replacement of specific amino acids within the TA of Gal4-Fis1p with proline can
826 lead to Gal4-mediated selectable marker activation. Strain MaV203 expressing Gal4-
827 Fis1p variants from plasmids b100 (WT), b188 (V134P), b189 (G137P), b129 (L139P),
828 b190 (A140P), b296 (A144P), or b101 (ΔTA) was cultured in SC-Trp medium then
829 spotted to SC-Trp or SMM-His + 20 mM 3-AT medium for 2 d. (B) TAs with specific
830 proline replacements can reduce mitochondrial targeting of a linked fluorescent
831 protein. Variants of the Fis1p TA fused to mCherry were expressed in WT strain
832 CDD961 from plasmids b109 (WT), b208 (V134P), b209 (G137P), b135 (L139P), b210
833 (A140P), b211 (A144P) and examined, along with mitochondria-targeted GFP, as in
834 Figure 2B. (C) Deletion of the Msp1p extractase does not allow tail-anchored proteins
835 mistargeted due to proline inclusion to return to mitochondria. Cells from
836 *msp1Δ/msp1Δ* strain CDD1044 expressing pHS1 and plasmids b109 (WT), b208
837 (V134P), b135 (L139P), b210 (A140P), or b211 (A144P) were inspected as in Figure 2B.
838 Scale bar, 5 μm.
839
840 **Figure 6**. Targeting of the Fis1p TA is not dependent upon a specific TA length. (A)
841 Deletion of up to three amino acids or insertion of up to three amino acids does not

842 allow Gal4-Fis1p to activate transcription. Mav203 cells expressing Gal4-Fis1p variants
843 from plasmids b229 (∇1A), b230 (∇2A), b231 (∇3A), b226 (ΔG136), b227 (ΔA135-G136),
844 b228 (ΔA135-G137), or b101 (ΔTA) were treated as in Figure 5A. (B) mCherry fused to a
845 Fis1p TA containing an insertion of up to three amino acids in length localizes properly
846 to mitochondria. Strain CDD961 expressing mCherry-TA fusions from plasmids b109
847 (WT), b235 (∇1A), b236 (∇2A), or b237 (∇3A) was visualized as in Figure 2B. (C)
848 mCherry fused to a Fis1p TA deleted of up to three amino acids is properly targeted to
849 mitochondria. Strain CDD961 expressing mCherry-TA fusions from plasmids b109
850 (WT), b232 (ΔG136), b233 (ΔA135-G136), or b234 (ΔA135-G137) was examined as in
851 Figure 2B. Scale bar, 5 μm.
852
853 **Figure 7.** The positively charged carboxyl-terminus of the Fis1p TA is important for
854 specific localization to the mitochondrial outer membrane. (A) Deletion of the final five
855 amino acids from the Fis1p TA permits transcriptional activation by Gal4-Fis1p. Strain
856 Mav203 harboring plasmids b100 (WT), b253 (R151X), or b101 (ΔTA) was treated as in
857 Figure 5A. (B) Removal of the last five amino acids from the Fis1p TA allows
858 mislocalization to the secretory system. Strain CDD961 expressing mCherry fused to
859 the WT Fis1p TA (b109) or expressing mCherry linked to a truncated Fis1p TA (R151X)
860 from plasmid b254 was evaluated as in Figure 2B. White arrowheads denote mCherry
861 localized to the nuclear envelope. Scale bar, 5 μm.
862
863 **Figure 8.** Negative charges allow higher transcriptional activity than positive charges
864 when placed at specific positions within the Gal4-Fis1p TA. Strain MaV203 was
865 transformed with plasmids pKS1 (vector), b100 (Gal4-Fis1), b101 [Gal4-Fis1(ΔTA)], or
866 plasmids encoding the indicated charge replacements within the Fis1p TA (plasmids
867 b173-b187 and b295). The resulting transformants were treated as in Figure 5A.
868
869 **Figure 9.** Fis1p TA targeting is hindered to a greater extent by inclusion of negatively
870 charged amino acids than by positively charged amino acids. (A) Examination of
871 mCherry-TA localization in WT cells expressing Msp1p. Strain CDD961 was

872 transformed with plasmids (b192-b207) expressing mCherry linked to the Fis1p TA
873 harboring the indicated substitutions. Cells were visualized as in Figure 2B. (B) Deletion
874 of Msp1p does not allow recovery of mitochondrial localization by poorly targeted
875 mCherry-TA variants. Strain CDD1044, deleted of Msp1p, was transformed with the
876 following plasmids encoding mCherry fused to the mutant TAs: b192 (V132D), b196
877 (A140D), b197 (A140E), b198 (A140K), b199 (A140R), b200 (A144D), b201 (A144E),
878 b134 (V145E), b204 (F148D), b205 (F148E). Transformants were examined as in Figure
879 2B. Scale bar, 5 μm.
880
881 **Figure 10.** Positive and negative charge replacements within the Fis1p TA can
882 generally support Fis1p function. (A) Normal mitochondrial morphology can be
883 maintained even when charges are placed within the hydrophobic MAD of the Fis1p
884 TA. Strain CDD741 was transformed with vector pRS313, a plasmid expressing WT
885 Fis1p (b239), or plasmids expressing Fis1p containing the indicated TA alterations
886 (plasmids b240-251). Mitochondrial morphology was visualized by expression of
887 mitochondria-targeted GFP from plasmid pHS12. Scale bar, 5 μm. (B) Induced, Fis1p-
888 dependent mitochondrial fragmentation is permitted by charge placement within the
889 Fis1p TA. Transformants analyzed in (A) were treated with sodium azide to provoke
890 mitochondrial fragmentation, and cells were scored for the maintenance of a
891 mitochondrial network (n=200 cells). (C) Charged residues within the TA provide exhibit
892 Fis1p activity during a genetic assay of Fis1p function. *fzo1Δ fis1Δ* strain CDD688,
893 carrying a CHX-counterselectable, *FZO1*-expressing plasmid, was transformed with
894 the *FIS1*-expressing plasmids enumerated above. After allowing cells to lose the *FZO1*-
895 encoding plasmid, serial dilutions were spotted to SLac-His containing 3 μg/mL CHX
896 to counterselect against *FZO1* expression ("lactate / no fusion") and incubated for 5 d
897 to test for maintenance of mtDNA. Cell proliferation indicates a lack of Fis1p activity.
898 To control for cell number spotted, cells from the same culture were placed on SMM-
899 Trp-His medium ("glucose / fusion") and incubated for 2 d.
900

901 **REFERENCES:**

902 Allen, R., Egan, B., Gabriel, K., Beilharz, T., and Lithgow, T. (2002). A conserved proline
903 residue is present in the transmembrane-spanning domain of Tom7 and other tail-
904 anchored protein subunits of the TOM translocase. FEBS Lett *514*, 347–350.

905 Araya, C. L., and Fowler, D. M. (2011). Deep mutational scanning: assessingprotein
906 function on a massive scale. Trends in Biotechnology *29*, 435–442.

907 Beilharz, T. (2003). Bipartite Signals Mediate Subcellular Targeting of Tail-anchored
908 Membrane Proteins in Saccharomyces cerevisiae. *278*, 8219–8223.

909 Borgese, N., Brambillasca, S., and Colombo, S. (2007). How tails guide tail-anchored
910 proteins to their destinations. Current Opinion in Cell Biology *19*, 368–375.

911 Borgese, N., Gazzoni, I., Barberi, M., Colombo, S., and Pedrazzini, E. (2001). Targeting
912 of a tail-anchored protein to endoplasmic reticulum and mitochondrial outer membrane
913 by independent but competing pathways. Mol Biol Cell *12*, 2482–2496.

914 Boucher, J. I., Cote, P., Flynn, J., Jiang, L., Laban, A., Mishra, P., Roscoe, B. P., and
915 Bolon, D. N. A. (2014). Viewing protein fitness landscapes through a next-gen lens.
916 Genetics *198*, 461–471.

917 Buchan, D. W. A., Minneci, F., Nugent, T. C. O., Bryson, K., and Jones, D. T. (2013).
918 Scalable web services for the PSIPRED Protein Analysis Workbench. Nucleic Acids
919 Res *41*, W349–W357.

920 Cartron, P.-F., Bellot, G., Oliver, L., Grandier-Vazeille, X., Manon, S., and Vallette, F. M.
921 (2008). Bax inserts into the mitochondrial outer membrane by different mechanisms.
922 FEBS Lett *582*, 3045–3051.

923 Chen, Y.-C., Umanah, G. K. E., Dephoure, N., Andrabi, S. A., Gygi, S. P., Dawson, T.
924 M., Dawson, V. L., and Rutter, J. (2014). Msp1/ATAD1 maintains mitochondrial function
925 by facilitating the degradation of mislocalized tail-anchored proteins. Embo J *33*, 1548–
926 1564.

927 Chou, P. Y., and Fasman, G. D. (1974). Conformational parameters for amino acids in
928 helical, beta-sheet, and random coil regions calculated from proteins. Biochemistry *13*,
929 211–222.

930 Colin, J., Garibal, J., Mignotte, B., and Guenal, I. (2009). The mitochondrial TOM
931 complex modulates bax-induced apoptosis in Drosophila. Biochemical and Biophysical
932 Research Communications *379*, 939–943.

933 Cymer, F., Heijne, von, G., and White, S. H. (2015). Mechanisms of Integral Membrane
934 Protein Insertion and Folding. J Mol Biol *427*, 999–1022.

935 de Mendoza, D., and Cronan, J. E., Jr. (1983). Thermal regulation of membrane lipid
936 fluidity in bacteria. Trends in Biochemical Sciences *8*, 49–52.

937 Denic, V., Dötsch, V., and Sinning, I. (2013). Endoplasmic reticulum targeting and
938 insertion of tail-anchored membrane proteins by the GET pathway. Cold Spring Harbor
939 Perspectives in Biology *5*, a013334–a013334.

940 Deshaies, R. J., and Schekman, R. (1987). A yeast mutant defective at an early stage in
941 import of secretory protein precursors into the endoplasmic reticulum. J Cell Biol *105*,
942 633–645.

943 Dong, H., Sharma, M., Zhou, H.-X., and Cross, T. A. (2012). Glycines: Role in α-Helical
944 Membrane Protein Structures and a Potential Indicator of Native Conformation.
945 Biochemistry *51*, 4779–4789.

946 Drozdetskiy, A., Cole, C., Procter, J., and Barton, G. J. (2015). JPred4: a protein
947 secondary structure prediction server. Nucleic Acids Res *43*, W389–W394.

948 Dufourc, E. J. (2008). Sterols and membrane dynamics. J Chem Biol *1*, 63–77.

949 Dunn, C. D., and Jensen, R. E. (2003). Suppression of a defect in mitochondrial protein
950 import identifies cytosolic proteins required for viability of yeast cells lacking
951 mitochondrial DNA. Genetics *165*, 35–45.

952 Durfee, T., Becherer, K., Chen, P. L., Yeh, S. H., Yang, Y., Kilburn, A. E., Lee, W. H.,
953 and Elledge, S. J. (1993). The retinoblastoma protein associates with the protein
954 phosphatase type 1 catalytic subunit. Genes Dev *7*, 555–569.

955 Edlich, F., Banerjee, S., Suzuki, M., Cleland, M. M., Arnoult, D., Wang, C., Neutzner, A.,
956 Tjandra, N., and Youle, R. J. (2011). Bcl-xL Retrotranslocates Bax from the
957 Mitochondria into the Cytosol. Cell *145*, 104–116.

958 Einerhand, A. W., Voorn-Brouwer, T. M., Erdmann, R., Kunau, W. H., and Tabak, H. F.
959 (1991). Regulation of transcription of the gene coding for peroxisomal 3-oxoacyl-CoA
960 thiolase of Saccharomcyes cerevisiae. European Journal of Biochemistry *200*, 113–
961 122.

962 Elazar, A., Weinstein, J., Biran, I., Fridman, Y., Bibi, E., and Fleishman, S. J. (2016).
963 Mutational scanning reveals the determinants of protein insertion and association
964 energetics in the plasma membrane. eLife *5*, 1302.

965 Engelman, D. M., and Steitz, T. A. (1981). The spontaneous insertion of proteins into
966 and across membranes: the helical hairpin hypothesis. Cell *23*, 411–422.

967 Fekkes, P., Shepard, K. A., and Yaffe, M. P. (2000). Gag3p, an outer membrane protein
968 required for fission of mitochondrial tubules. J Cell Biol *151*, 333–340.

969 Fowler, D. M., and Fields, S. (2014). Deep mutational scanning: a new style of protein
970 science. Nature Publishing Group *11*, 801–807.

971 Förtsch, J., Hummel, E., Krist, M., and Westermann, B. (2011). The myosin-related
972 motor protein Myo2 is an essential mediator of bud-directed mitochondrial movement
973 in yeast. J Cell Biol *194*, 473–488.

974 Garipler, G., Mutlu, N., Lack, N. A., and Dunn, C. D. (2014). Deletion of conserved
975 protein phosphatases reverses defects associated with mitochondrial DNA damage in
976 Saccharomyces cerevisiae. Proceedings of the National Academy of Sciences *111*,
977 1473–1478.

978 Gimpelev, M., Forrest, L. R., Murray, D., and Honig, B. (2004). Helical Packing Patterns
979 in Membrane and Soluble Proteins. Biophysical Journal *87*, 4075–4086.

980 Goecks, J., Nekrutenko, A., Taylor, J., Galaxy Team (2010). Galaxy: a comprehensive
981 approach for supporting accessible, reproducible, and transparent computational
982 research in the life sciences. Genome Biol *11*, R86.

983 Gross, A., Pilcher, K., Blachly-Dyson, E., Basso, E., Jockel, J., Bassik, M. C.,
984 Korsmeyer, S. J., and Forte, M. (2000). Biochemical and Genetic Analysis of the
985 Mitochondrial Response of Yeast to BAX and BCL-XL. Mol Cell Biol *20*, 3125–3136.

986 Habib, S. J., Vasiljev, A., Neupert, W., and Rapaport, D. (2003). Multiple functions of
987 tail-anchor domains of mitochondrial outer membrane proteins. FEBS Lett *555*, 511–
988 515.

989 He, S., and Fox, T. D. (1999). Mutations affecting a yeast mitochondrial inner
990 membrane protein, pnt1p, block export of a mitochondrially synthesized fusion protein
991 from the matrix. Mol Cell Biol *19*, 6598–6607.

992 Hermann, G. J., Thatcher, J. W., Mills, J. P., Hales, K. G., Fuller, M. T., Nunnari, J., and
993 Shaw, J. M. (1998). Mitochondrial fusion in yeast requires the transmembrane GTPase
994 Fzo1p. J Cell Biol *143*, 359–373.

995 Hietpas, R. T., Jensen, J. D., and Bolon, D. N. A. (2011). Experimental illumination of a
996 fitness landscape. Proceedings of the National Academy of Sciences *108*, 7896–7901.

997 Honig, B. H., and Hubbell, W. L. (1984). Stability of “salt bridges” in membrane
998 proteins. Proc Natl Acad Sci USA *81*, 5412–5416.

999 Horie, C., Suzuki, H., Sakaguchi, M., and Mihara, K. (2002). Characterization of signal
1000 that directs C-tail-anchored proteins to mammalian mitochondrial outer membrane.
1001 Mol Biol Cell *13*, 1615–1625.

1002 Horie, C., Suzuki, H., Sakaguchi, M., and Mihara, K. (2003). Targeting and assembly of
1003 mitochondrial tail-anchored protein Tom5 to the TOM complex depend on a signal

1004 distinct from that of tail-anchored proteins dispersed in the membrane. J Biol Chem
1005 *278*, 41462–41471.

1006 Isenmann, S., Khew-Goodall, Y., Gamble, J., Vadas, M., and Wattenberg, B. W. (1998).
1007 A splice-isoform of vesicle-associated membrane protein-1 (VAMP-1) contains a
1008 mitochondrial targeting signal. Mol Biol Cell *9*, 1649–1660.

1009 Itakura, E., Zavodszky, E., Shao, S., Wohlever, M. L., Keenan, R. J., and Hegde, R. S.
1010 (2016). Ubiquilins Chaperone and Triage Mitochondrial Membrane Proteins for
1011 Degradation. Molecular Cell, 1–14.

1012 Jensen, R. E., Schmidt, S., and Mark, R. J. (1992). Mutations in a 19-amino-acid
1013 hydrophobic region of the yeast cytochrome c1 presequence prevent sorting to the
1014 mitochondrial intermembrane space. Mol Cell Biol *12*, 4677–4686.

1015 Johnson, N., Powis, K., and High, S. (2013). Post-translational translocation into the
1016 endoplasmic reticulum. BBA-Molecular Cell Research *1833*, 2403–2409.

1017 Kemper, C., Habib, S. J., Engl, G., Heckmeyer, P., Dimmer, K. S., and Rapaport, D.
1018 (2008). Integration of tail-anchored proteins into the mitochondrial outer membrane
1019 does not require any known import components. Journal of Cell Science *121*, 1990–
1020 1998.

1021 Kim, C., Schmidt, T., Cho, E.-G., Ye, F., Ulmer, T. S., and Ginsberg, M. H. (2012). Basic
1022 amino-acid side chains regulate transmembrane integrin signalling. Nature *481*, 209–
1023 213.

1024 Klecker, T., Wemmer, M., Haag, M., Weig, A., Böckler, S., Langer, T., Nunnari, J., and
1025 Westermann, B. (2015). Interaction of MDM33 with mitochondrial inner membrane
1026 homeostasis pathways in yeast. Sci. Rep., 1–14.

1027 Koch, A., Yoon, Y., Bonekamp, N. A., McNiven, M. A., and Schrader, M. (2005). A role
1028 for Fis1 in both mitochondrial and peroxisomal fission in mammalian cells. Mol Biol Cell
1029 *16*, 5077–5086.

1030 Krumpe, K., Frumkin, I., Herzig, Y., Rimon, N., Özbalci, C., Brügger, B., Rapaport, D.,
1031 and Schuldiner, M. (2012). Ergosterol content specifies targeting of tail-anchored
1032 proteins to mitochondrial outer membranes. Mol Biol Cell *23*, 3927–3935.

1033 Kuravi, K., Nagotu, S., Krikken, A. M., Sjollema, K., Deckers, M., Erdmann, R.,
1034 Veenhuis, M., and van der Klei, I. J. (2006). Dynamin-related proteins Vps1p and
1035 Dnm1p control peroxisome abundance in Saccharomyces cerevisiae. Journal of Cell
1036 Science *119*, 3994–4001.

1037 Kuroda, R., Ikenoue, T., Honsho, M., Tsujimoto, S., Mitoma, J. Y., and Ito, A. (1998).
1038 Charged amino acids at the carboxyl-terminal portions determine the intracellular
1039 locations of two isoforms of cytochrome b5. J Biol Chem *273*, 31097–31102.

1040 Lee, J., Kim, D. H., and Hwang, I. (2014). Specific targeting of proteins to outer
1041 envelope membranes of endosymbiotic organelles, chloroplasts, and mitochondria.
1042 Front Plant Sci *5*, 173.

1043 Lee, S., Lim, W. A., and Thorn, K. S. (2013). Improved blue, green, and red fluorescent
1044 protein tagging vectors for S. cerevisiae. PLoS ONE *8*, e67902.

1045 Li, S. C., Goto, N. K., Williams, K. A., and Deber, C. M. (1996). Alpha-helical, but not
1046 beta-sheet, propensity of proline is determined by peptide environment. Proc Natl
1047 Acad Sci USA *93*, 6676–6681.

1048 Long, S. B., Campbell, E. B., and MacKinnon, R. (2005). Voltage Sensor of Kv1.2:
1049 Structural Basis of Electromechanical Coupling. Science *309*, 903–908.

1050 Maarse, A. C., Blom, J., Grivell, L. A., and Meijer, M. (1992). MPI1, an essential gene
1051 encoding a mitochondrial membrane protein, is possibly involved in protein import into
1052 yeast mitochondria. Embo J *11*, 3619–3628.

1053 Masella, A. P., Bartram, A. K., Truszkowski, J. M., Brown, D. G., and Neufeld, J. D.
1054 (2012). PANDAseq: paired-end assembler for illumina sequences. BMC Bioinformatics
1055 *13*, 31.

1056 Melamed, D., Young, D. L., Gamble, C. E., Miller, C. R., and Fields, S. (2013). Deep
1057 mutational scanning of an RRM domain of the Saccharomyces cerevisiae poly(A)-
1058 binding protein. Rna *19*, 1537–1551.

1059 Meyers, S., Schauer, W., Balzi, E., Wagner, M., Goffeau, A., and Golin, J. (1992).
1060 Interaction of the yeast pleiotropic drug resistance genes PDR1 and PDR5. Curr Genet
1061 *21*, 431–436.

1062 Monné, M., Nilsson, I., Johansson, M., Elmhed, N., and Heijne, von, G. (1998).
1063 Positively and negatively charged residues have different effects on the position in the
1064 membrane of a model transmembrane helix. J Mol Biol *284*, 1177–1183.

1065 Mozdy, A. D., McCaffery, J. M., and Shaw, J. M. (2000). Dnm1p GTPase-mediated
1066 mitochondrial fission is a multi-step process requiring the novel integral membrane
1067 component Fis1p. J Cell Biol *151*, 367–380.

1068 Mutlu, N., Garipler, G., Akdoğan, E., and Dunn, C. D. (2014). Activation of the
1069 pleiotropic drug resistance pathway can promote mitochondrial DNA retention by
1070 fusion-defective mitochondria in Saccharomyces cerevisiae. G3 (Bethesda) *4*, 1247–
1071 1258.

1072 Nechushtan, A., Smith, C. L., Hsu, Y. T., and Youle, R. J. (1999). Conformation of the
1073 Bax C-terminus regulates subcellular location and cell death. Embo J *18*, 2330–2341.

1074 Neupert, W. (2015). A Perspective on Transport of Proteins into Mitochondria: A Myriad

1075 of Open Questions. J Mol Biol *427*, 1135–1158.

1076 O'Neil, K. T., and DeGrado, W. F. (1990). A thermodynamic scale for the helix-forming
1077 tendencies of the commonly occurring amino acids. Science *250*, 646–651.

1078 Okreglak, V., and Walter, P. (2014). The conserved AAA-ATPase Msp1 confers
1079 organelle specificity to tail-anchored proteins. Proceedings of the National Academy of
1080 Sciences *111*, 8019–8024.

1081 Oldenburg, K. R., Vo, K. T., Michaelis, S., and Paddon, C. (1997). Recombination-
1082 mediated PCR-directed plasmid construction in vivo in yeast. Nucleic Acids Res *25*,
1083 451–452.

1084 Ott, M., Norberg, E., Walter, K. M., Schreiner, P., Kemper, C., Rapaport, D.,
1085 Zhivotovsky, B., and Orrenius, S. (2007). The mitochondrial TOM complex is required
1086 for tBid/Bax-induced cytochrome c release. J Biol Chem *282*, 27633–27639.

1087 Parsegian, A. (1969). Energy of an ion crossing a low dielectric membrane: solutions to
1088 four relevant electrostatic problems. Nature *221*, 844–846.

1089 Pavlidis, P., and Noble, W. S. (2003). Matrix2png: a utility for visualizing matrix data.
1090 Bioinformatics *19*, 295–296.

1091 Pédelacq, J.-D., Cabantous, S., Tran, T., Terwilliger, T. C., and Waldo, G. S. (2005).
1092 Engineering and characterization of a superfolder green fluorescent protein. Nat
1093 Biotechnol *24*, 79–88.

1094 Ping, H. A., Kraft, L. M., Chen, W., Nilles, A. E., and Lackner, L. L. (2016). Num1
1095 anchors mitochondria to the plasma membrane via two domains with different lipid
1096 binding specificities. J Cell Biol *266*, jcb.201511021–12.

1097 Prasad, R., and Goffeau, A. (2012). Yeast ATP-Binding Cassette Transporters
1098 Conferring Multidrug Resistance. Annu. Rev. Microbiol. *66*, 39–63.

1099 Rapaport, D. (2003). Finding the right organelle. Targeting signals in mitochondrial
1100 outer-membrane proteins. EMBO Rep *4*, 948–952.

1101 Rapaport, D., Brunner, M., Neupert, W., and Westermann, B. (1998). Fzo1p is a
1102 mitochondrial outer membrane protein essential for the biogenesis of functional
1103 mitochondria in Saccharomyces cerevisiae. J Biol Chem *273*, 20150–20155.

1104 Robinson, J. S., Klionsky, D. J., Banta, L. M., and Emr, S. D. (1988). Protein sorting in
1105 Saccharomyces cerevisiae: isolation of mutants defective in the delivery and
1106 processing of multiple vacuolar hydrolases. Mol Cell Biol *8*, 4936–4948.

1107 Russ, W. P., and Engelman, D. M. (2000). The GxxxG motif: A framework for
1108 transmembrane helix-helix association. J Mol Biol *296*, 911–919.

1109 Ryan, K. R., Leung, R. S., and Jensen, R. E. (1998). Characterization of the
1110 mitochondrial inner membrane translocase complex: the Tim23p hydrophobic domain
1111 interacts with Tim17p but not with other Tim23p molecules. Mol Cell Biol *18*, 178–187.

1112 Sapay, N., Guermeur, Y., and Deléage, G. (2006). BMC Bioinformatics. BMC
1113 Bioinformatics *7*, 255–11.

1114 Schellenberg, B. *et al.* (2013). Bax Exists in a Dynamic Equilibrium between the Cytosol
1115 and Mitochondria to Control Apoptotic Priming. Molecular Cell *49*, 959–971.

1116 Schinzel, A., Kaufmann, T., Schuler, M., Martinalbo, J., Grubb, D., and Borner, C.
1117 (2004). Conformational control of Bax localization and apoptotic activity by Pro168. J
1118 Cell Biol *164*, 1021–1032.

1119 Schow, E. V., Freites, J. A., Cheng, P., Bernsel, A., Heijne, von, G., White, S. H., and
1120 Tobias, D. J. (2010). Arginine in Membranes: The Connection Between Molecular
1121 Dynamics Simulations and Translocon-Mediated Insertion Experiments. J Membrane
1122 Biol *239*, 35–48.

1123 Schuldiner, M., Metz, J., Schmid, V., Denic, V., Rakwalska, M., Schmitt, H. D.,
1124 Schwappach, B., and Weissman, J. S. (2008). The GET Complex Mediates Insertion of
1125 Tail-Anchored Proteins into the ER Membrane. Cell *134*, 634–645.

1126 Segrest, J. P., De Loof, H., Dohlman, J. G., Brouillette, C. G., and Anantharamaiah, G.
1127 M. (1990). Amphipathic helix motif: Classes and properties. Proteins: Structure,
1128 Function, and Bioinformatics *8*, 103–117.

1129 Senes, A., Engel, D. E., and DeGrado, W. F. (2004). Folding of helical membrane
1130 proteins: the role of polar, GxxxG-like and proline motifs. Current Opinion in Structural
1131 Biology *14*, 465–479.

1132 Sesaki, H., and Jensen, R. E. (1999). Division versus fusion: Dnm1p and Fzo1p
1133 antagonistically regulate mitochondrial shape. J Cell Biol *147*, 699–706.

1134 Setoguchi, K., Otera, H., and Mihara, K. (2006). Cytosolic factor- and TOM-
1135 independent import of C-tail-anchored mitochondrial outer membrane proteins. Embo
1136 J *25*, 5635–5647.

1137 Sikorski, R. S., and Hieter, P. (1989). A system of shuttle vectors and yeast host strains
1138 designed for efficient manipulation of DNA in Saccharomyces cerevisiae. Genetics *122*,
1139 19–27.

1140 Sinzel, M., Tan, T., Wendling, P., Kalbacher, H., Özbalci, C., Chelius, X., Westermann,
1141 B., Brügger, B., Rapaport, D., and Dimmer, K. S. (2016). Mcp3 is a novel mitochondrial
1142 outer membrane protein that follows a unique IMP-dependent biogenesis pathway.
1143 EMBO Rep *17*, 965–981.

1144 Starita, L. M., Young, D. L., Islam, M., Kitzman, J. O., Gullingsrud, J., Hause, R. J.,
1145 Fowler, D. M., Parvin, J. D., Shendure, J., and Fields, S. (2015). Massively Parallel
1146 Functional Analysis of BRCA1 RING Domain Variants. Genetics *200*, 413–422.

1147 Stirling, C. J., Rothblatt, J., Hosobuchi, M., Deshaies, R., and Schekman, R. (1992).
1148 Protein translocation mutants defective in the insertion of integral membrane proteins
1149 into the endoplasmic reticulum. Mol Biol Cell *3*, 129–142.

1150 Stojanovski, D., Guiard, B., Kozjak-Pavlovic, V., Pfanner, N., and Meisinger, C. (2007).
1151 Alternative function for the mitochondrial SAM complex in biogenesis of alpha-helical
1152 TOM proteins. J Cell Biol *179*, 881–893.

1153 Stojanovski, D., Koutsopoulos, O. S., Okamoto, K., and Ryan, M. T. (2004). Levels of
1154 human Fis1 at the mitochondrial outer membrane regulate mitochondrial morphology.
1155 Journal of Cell Science *117*, 1201–1210.

1156 Strandberg, E., and Killian, J. A. (2003). Snorkeling of lysine side chains in
1157 transmembrane helices: how easy can it get? FEBS Lett *544*, 69–73.

1158 Suzuki, M., Jeong, S. Y., Karbowski, M., Youle, R. J., and Tjandra, N. (2003). The
1159 solution structure of human mitochondria fission protein Fis1 reveals a novel TPR-like
1160 helix bundle. J Mol Biol *334*, 445–458.

1161 Taxis, C., and Knop, M. (2006). System of centromeric, episomal, and integrative
1162 vectors based on drug resistance markers for Saccharomyces cerevisiae.

1163 Tieu, Q., and Nunnari, J. (2000). Mdv1p is a WD repeat protein that interacts with the
1164 dynamin-related GTPase, Dnm1p, to trigger mitochondrial division. J Cell Biol *151*,
1165 353–366.

1166 Van der Leij, I., Franse, M. M., Elgersma, Y., Distel, B., and Tabak, H. F. (1993). PAS10
1167 is a tetratricopeptide-repeat protein that is essential for the import of most matrix
1168 proteins into peroxisomes of Saccharomyces cerevisiae. Proc Natl Acad Sci USA *90*,
1169 11782–11786.

1170 Vidal, M., Brachmann, R. K., Fattaey, A., Harlow, E., and Boeke, J. D. (1996a). Reverse
1171 two-hybrid and one-hybrid systems to detect dissociation of protein-protein and DNA-
1172 protein interactions. Proc Natl Acad Sci USA *93*, 10315–10320.

1173 Vidal, M., Braun, P., Chen, E., Boeke, J. D., and Harlow, E. (1996b). Genetic
1174 characterization of a mammalian protein-protein interaction domain by using a yeast
1175 reverse two-hybrid system. Proc Natl Acad Sci USA *93*, 10321–10326.

1176 Voss, N. R., Gerstein, M., Steitz, T. A., and Moore, P. B. (2006). The Geometry of the
1177 Ribosomal Polypeptide Exit Tunnel. J Mol Biol *360*, 893–906.

1178 Wattenberg, B. W., Clark, D., and Brock, S. (2007). An artificial mitochondrial tail

1179 signal/anchor sequence confirms a requirement for moderate hydrophobicity for
1180 targeting. Biosci Rep *27*, 385–401.

1181 Wattenberg, B., and Lithgow, T. (2001). Targeting of C-terminal (tail)-anchored
1182 proteins: understanding how cytoplasmic activities are anchored to intracellular
1183 membranes. Traffic *2*, 66–71.

1184 Wells, R. C., and Hill, R. B. (2011). The cytosolic domain of Fis1 binds and reversibly
1185 clusters lipid vesicles. PLoS ONE *6*, e21384.

1186 Yoon, Y., Krueger, E. W., Oswald, B. J., and McNiven, M. A. (2003). The mitochondrial
1187 protein hFis1 regulates mitochondrial fission in mammalian cells through an interaction
1188 with the dynamin-like protein DLP1. Mol Cell Biol *23*, 5409–5420.

1189 Yu, C.-H., Dang, Y., Zhou, Z., Wu, C., Zhao, F., Sachs, M. S., and Liu, Y. (2015). Codon
1190 Usage Influences the Local Rate of Translation Elongation to Regulate Co-translational
1191 Protein Folding. Molecular Cell *59*, 744–754.

1192

1193

1194 **SUPPLEMENTAL FIGURE AND TABLE LEGENDS:**

1195

1196 **Figure S1.** A Gal4-Fis1 fusion localizes to mitochondria. *fis1Δ* strain CDD692 was
1197 transformed with plasmid b102, expressing a Gal4-Fis1p construct also harboring a
1198 central sfGFP domain from a high-copy plasmid. Mitochondrial DNA of live cells was
1199 stained with DAPI to reveal mitochondrial location. -located DNA and visualized by
1200 fluorescence microscopy. Scale bar, 5 μm.

1201

1202 **Figure S2.** Fusion to the Fis1p TA constrains Pdr1p activity. Strain BY4743 was
1203 transformed with plasmid b158 [Pdr1-Fis1(TA) WT], b159 [Pdr1-Fis1(TA) V145E], b160
1204 [Pdr1-249-Fis1(TA) WT], b165 [Pdr1-249-Fis1(TA) V145E], or empty vector pRS316.
1205 Cells were cultured in SC-Ura medium, then spotted to SC-Ura medium or SC-Ura
1206 medium containing 0.2 μg/ml CHX and incubated for 2 d.

1207

1208 **Figure S3.** An examination of amino acid replacement representation within the Fis1p
1209 TA library. The fraction of counts representing each amino acid replacement in the
1210 starting SC-Trp library (fObs) was compared to the fraction that would be expected
1211 based on randomized codon recovery (fExp). Native amino acids are represented by a
1212 black square with a blue dot. Amino acid replacements with no representation in the
1213 library are represented by empty black squares. The predicted MAD is indicated by a
1214 red line.

1215

1216 **Figure S4.** Amino acid replacement frequencies within the Fis1p TA suggest that
1217 assessing histidine auxotrophy in the presence of 3-AT may provide the most
1218 informative results regarding Gal4-Fis1p location. Quantification of replacement in
1219 SMM-Trp-His medium without 3-AT (A), containing 5 mM 3-AT (B), containing 10mM 3-
1220 AT (C), or in SC-Ura medium (D). In all panels, black outlines indicate the native amino
1221 acid at each position within the Fis1p TA. Amino acid replacements not detectable
1222 under selective conditions are denoted by black, filled squares. The predicted MAD is
1223 indicated by a red line.

1224

1225

1226 **Figure S5.** Little evidence exists for codon-level control of Gal4-Fis1p TA targeting.
1227 The $\log_2$ of enrichment values for each codon following selection of the Fis1p TA library
1228 in SMM-Trp-His medium containing 20 mM 3-AT are illustrated. Green outlines denote
1229 the native amino acid at each position. Codon replacements with no representation in
1230 the library following selection are represented by empty black squares. The predicted
1231 MAD is indicated by a red line.

1232

1233 **Figure S6.** Uracil auxotrophy tests that were performed alongside histidine auxotrophy
1234 tests. Samples cultured in SC-Trp for (A) Figure 5A, (B) Figure 6A, (C) Figure 7A, and
1235 (D) Figure 8 were also spotted to SC-Ura medium and incubated for 2 d.

1236

1237 **Figure S7.** mCherry fused to Fis1p TAs of varying length remains targeted to the ER in
1238 *spf1Δ* mutant cells. (A) Strain CDD1031, lacking Spf1p and expressing mCherry-TA
1239 fusions from plasmids b109 (WT), b235 (∇1A), b236 (∇2A), or b237 (∇3A), b232
1240 (ΔG136), b233 (ΔA135-G136), or b234 (ΔA135-G137) were examined as in Figure 2B.
1241 White arrowheads denote mCherry localized to the nuclear envelope. Scale bar, 5 μm.

1242

1243 **Figure S8.** A mutated Fis1p TA lacking the positively charged carboxyl-terminus
1244 localizes to the ER independent of Get3p expression. *get3Δ/get3Δ* strain CDD1033
1245 expressing mCherry fused to a WT Fis1p TA from plasmid b109 or expressing mCherry
1246 fused to a Fis1p TA lacking the positively charged carboxyl-terminus (R151X) from
1247 plasmid b254 were examined as in Figure 2B. Mitochondria were labelled with GFP
1248 expressed from pHS1. White arrowheads denote mCherry localized to the nuclear
1249 envelope. Scale bar, 5 μm.

1250

1251 **Figure S9.** The TAs of human proteins do not universally target to mitochondria in
1252 yeast. (A) The hFIS1 TA is mistargeted to the ER in *S. cerevisiae*. Strain CDD961
1253 containing plasmid b257 expressing mCherry fused to the hFIS1 TA was analyzed as in

1254 Figure 2B. (B) The hFIS1 TA does not permit activity of a fused Gal4p within the
1255 nucleus. Strain MaV203 was transformed with plasmid b100 (Gal4-Fis1), b258 [Gal4-
1256 hFIS1(TA)], or plasmid b101 (Gal4-Fis1ΔTA) and assessed as in Figure 5A. (C) The BAX
1257 TA can target to mitochondria in *S. cerevisiae*. Strain CDD961 transformed with
1258 plasmid b255, which expresses mCherry fused to the BAX TA, was examined as in
1259 Figure 2B. Scale bar, 5 μm.
1260
1261 **Figure S10.** Temperature affects the outcome of adding a positive charge to the Fis1p
1262 TA. Samples used in Figure 8 were also spotted to SMM-His medium containing 20
1263 mM 3-AT and incubated at 18˚C for 4 d (A) or 37˚C for 3 d (B).
1264
1265 **Figure S11.** Most charge replacements within the Fis1p MAD permit Fis1p-dependent
1266 mitochondrial fragmentation. Images of azide-treated cells examined in Figure 10B are
1267 provided. Scale bar, 5 μm.
1268
1269 **Table S1.** Tail anchor sequence counts from individual pools.
1270
1271 **Table S2.** Strains used during this study.
1272
1273 **Table S3.** Plasmids used for experiments during this study.
1274
1275 **Table S4.** Oligonucleotides used in this study.
1276
1277
1278
1279
1280
1281
1282
1283

A

mitochondrial outer membrane

Gal4-Fis1 fusion

mutations in the Fis1 TA
allow movement to the nucleus
and activation of selectable markers

nucleus

Gal4-Fis1 fusion

HIS3
URA3

Gal4-responsive promoter

B

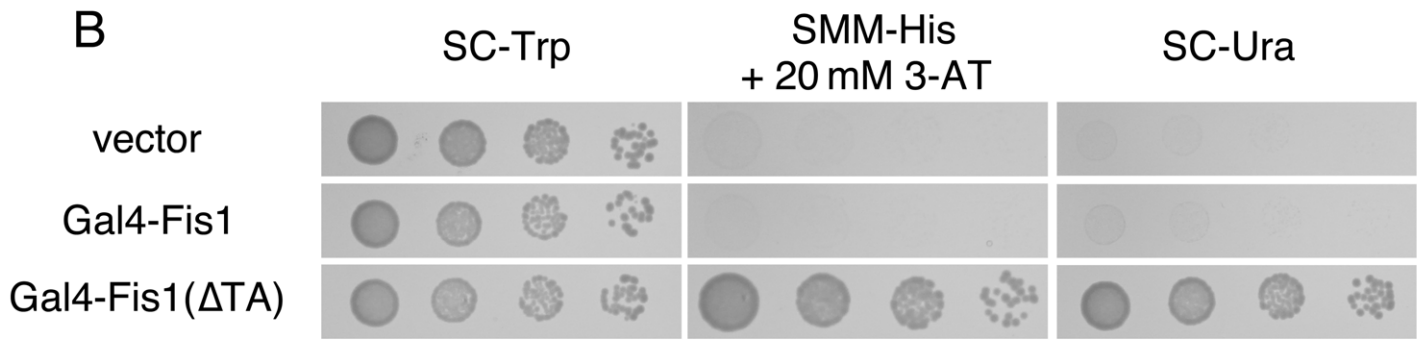

Figure 1

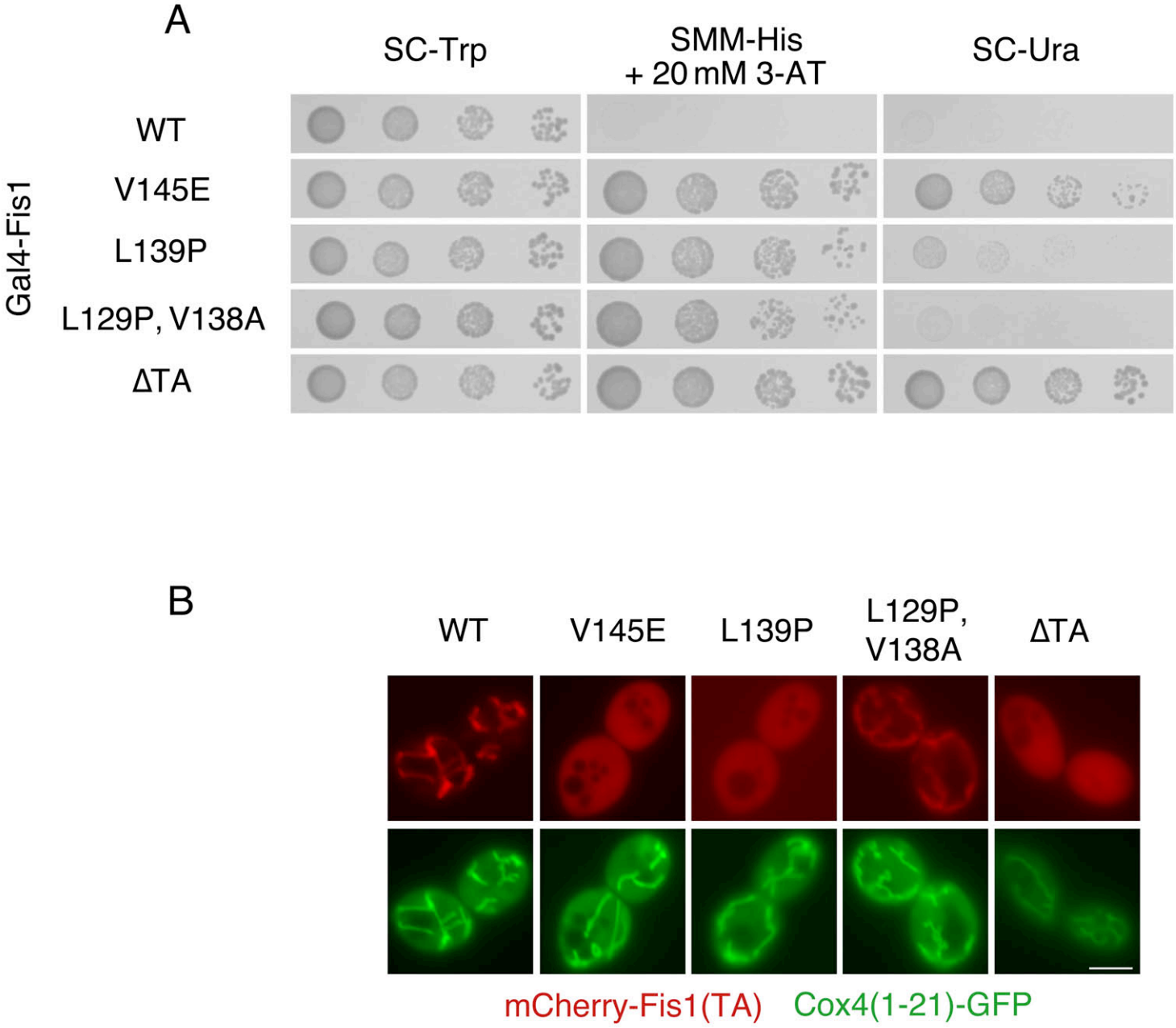
A
SC-Trp
SMM-His
+ 20 mM 3-AT
SC-Ura
Gal4-Fis1
WT
V145E
L139P
L129P, V138A
ΔTA
B
WT
V145E
L139P
L129P,
V138A
ΔTA
mCherry-Fis1(TA)
Cox4(1-21)-GFP

Figure 2

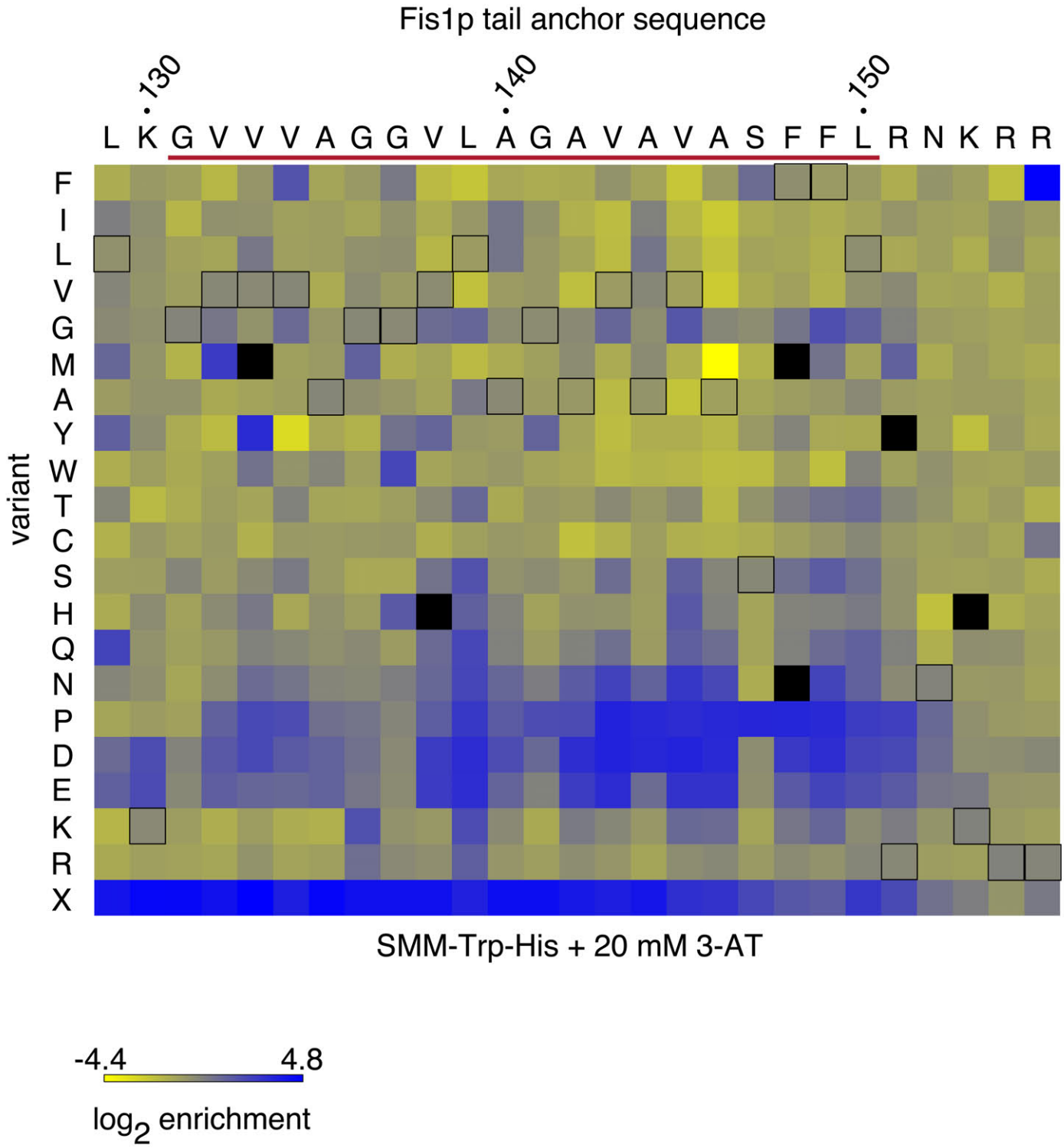
Fis1p tail anchor sequence
130
140
150
L K G V V V A G G V L A G A V A V A S F F L R N K R R
variant
F
I
L
V
G
M
A
Y
W
T
C
S
H
Q
N
P
D
E
K
R
X
SMM-Trp-His + 20 mM 3-AT
-4.4
4.8
log2 enrichment

Figure 3

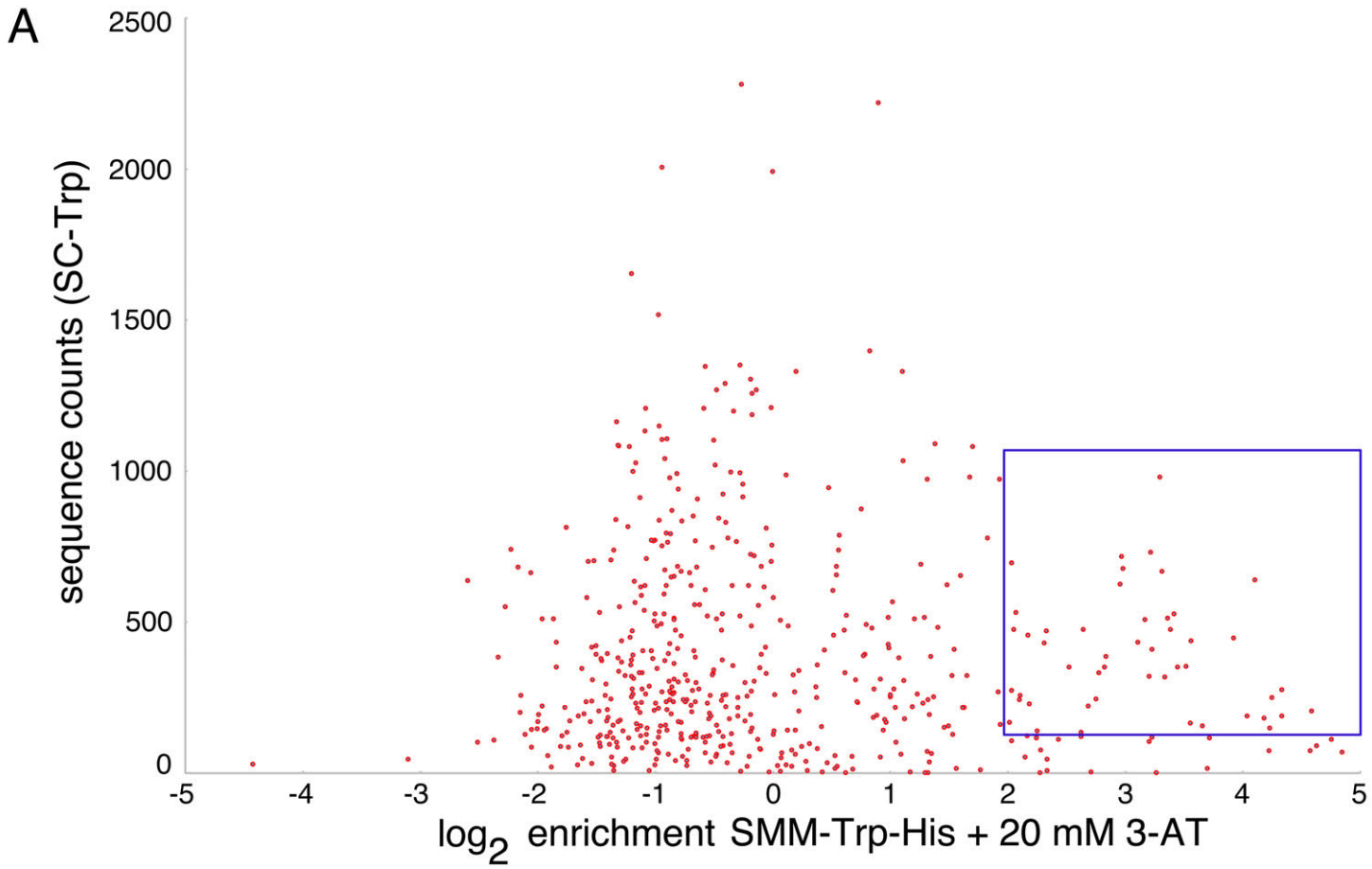
A
sequence counts (SC-Trp)
2500
2000
1500
1000
500
0
-5
-4
-3
-2
-1
0
1
2
3
4
5
log2 enrichment SMM-Trp-His + 20 mM 3-AT

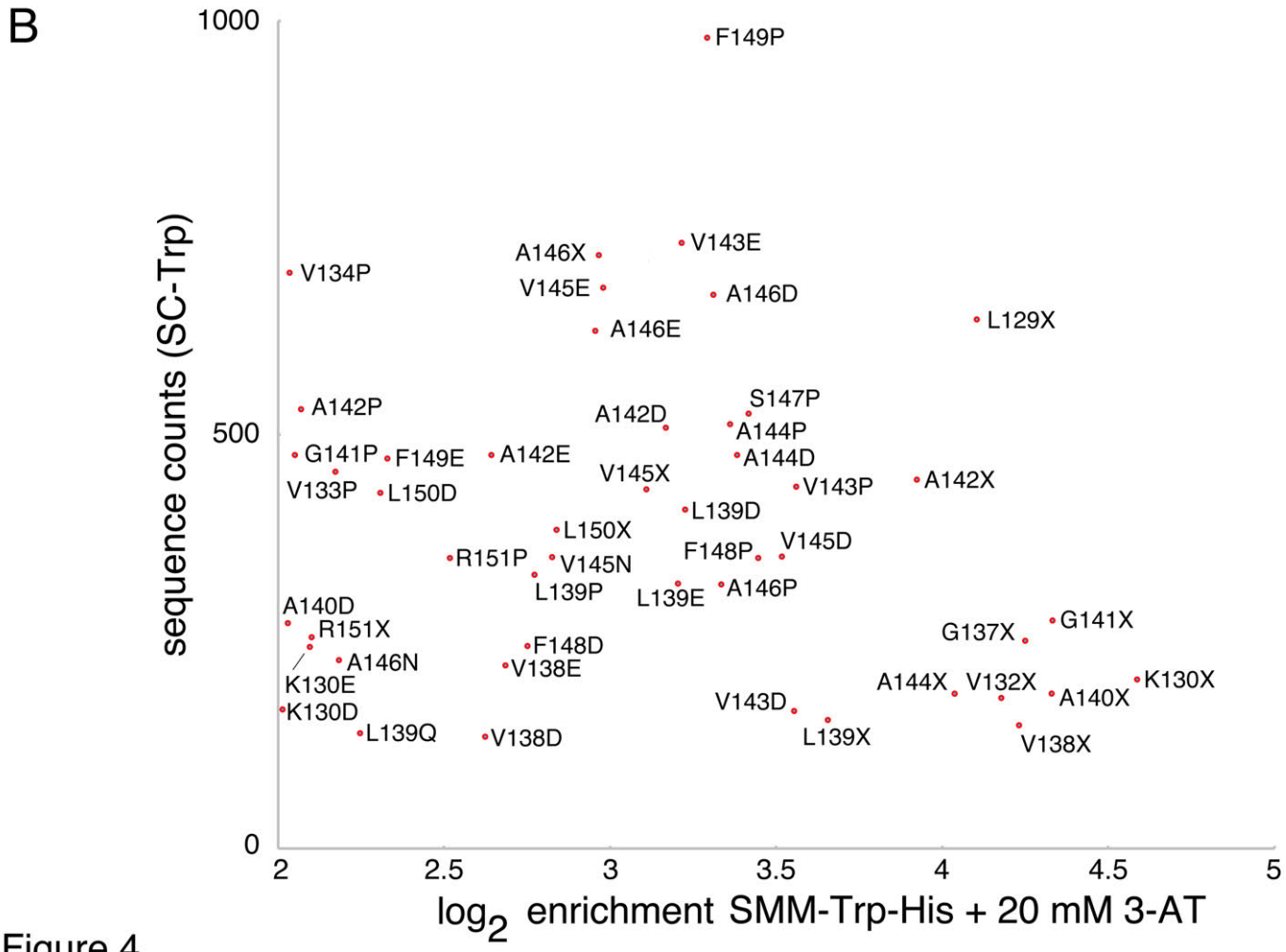
B
sequence counts (SC-Trp)
1000
500
0
2
2.5
3
3.5
4
4.5
5
log2 enrichment SMM-Trp-His + 20 mM 3-AT
F149P
V143E
A146X
V134P
V145E
A146D
A146E
L129X
A142P
S147P
A142D
A144P
G141P
F149E
A142E
A144D
V145X
V133P
L150D
V143P
A142X
L139D
L150X
V145D
R151P
V145N
F148P
L139P
L139E
A146P
A140D
R151X
G137X
G141X
F148D
A146N
V138E
K130E
A144X
V132X
K130X
A140X
V143D
K130D
L139Q
V138D
L139X
V138X

Figure 4

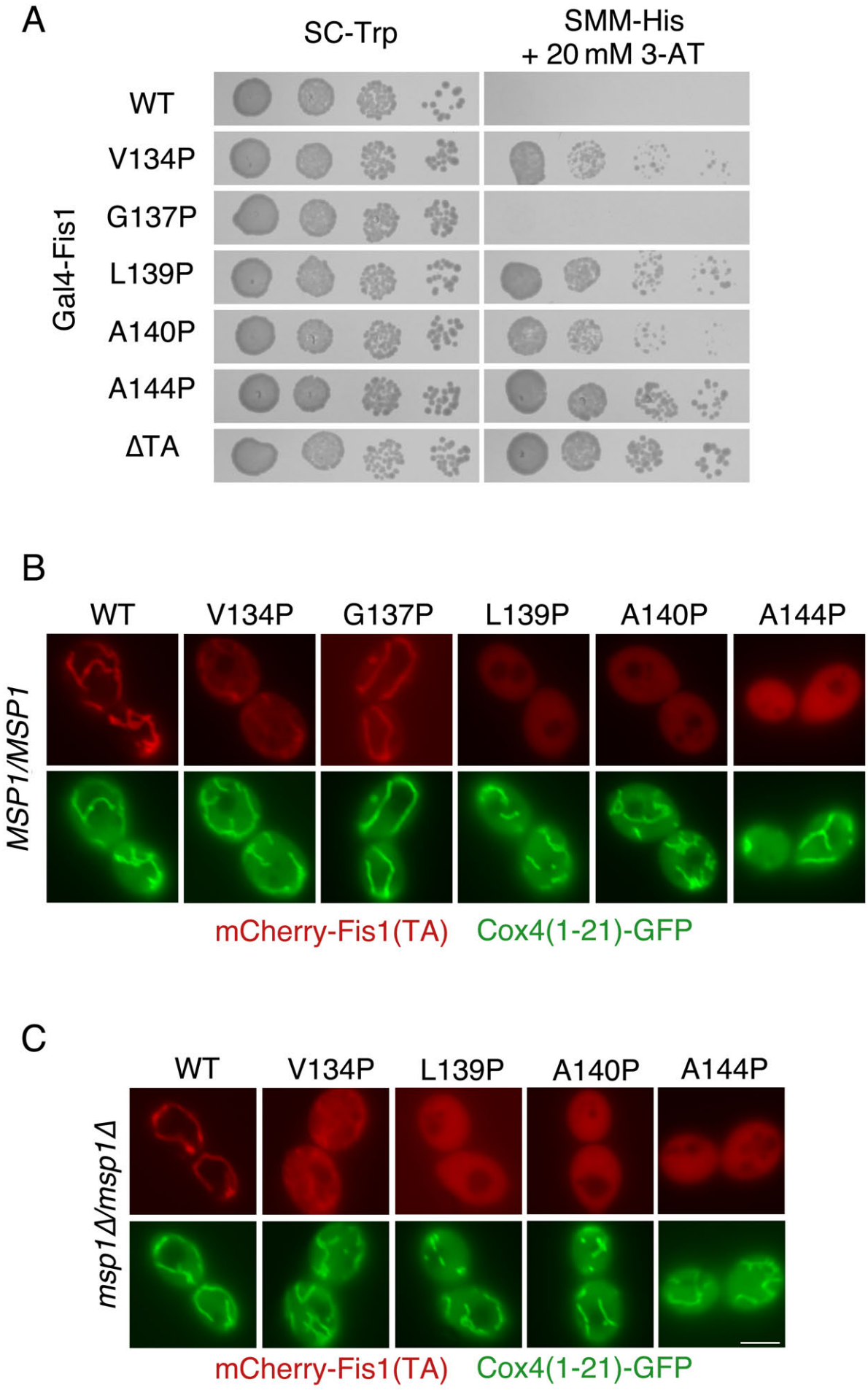
A
SC-Trp
SMM-His
+ 20 mM 3-AT
Gal4-Fis1
WT
V134P
G137P
L139P
A140P
A144P
ΔTA
B
WT
V134P
G137P
L139P
A140P
A144P
MSP1/MSP1
mCherry-Fis1(TA)
Cox4(1-21)-GFP
C
WT
V134P
L139P
A140P
A144P
msp1Δ/msp1Δ
mCherry-Fis1(TA)
Cox4(1-21)-GFP

Figure 5

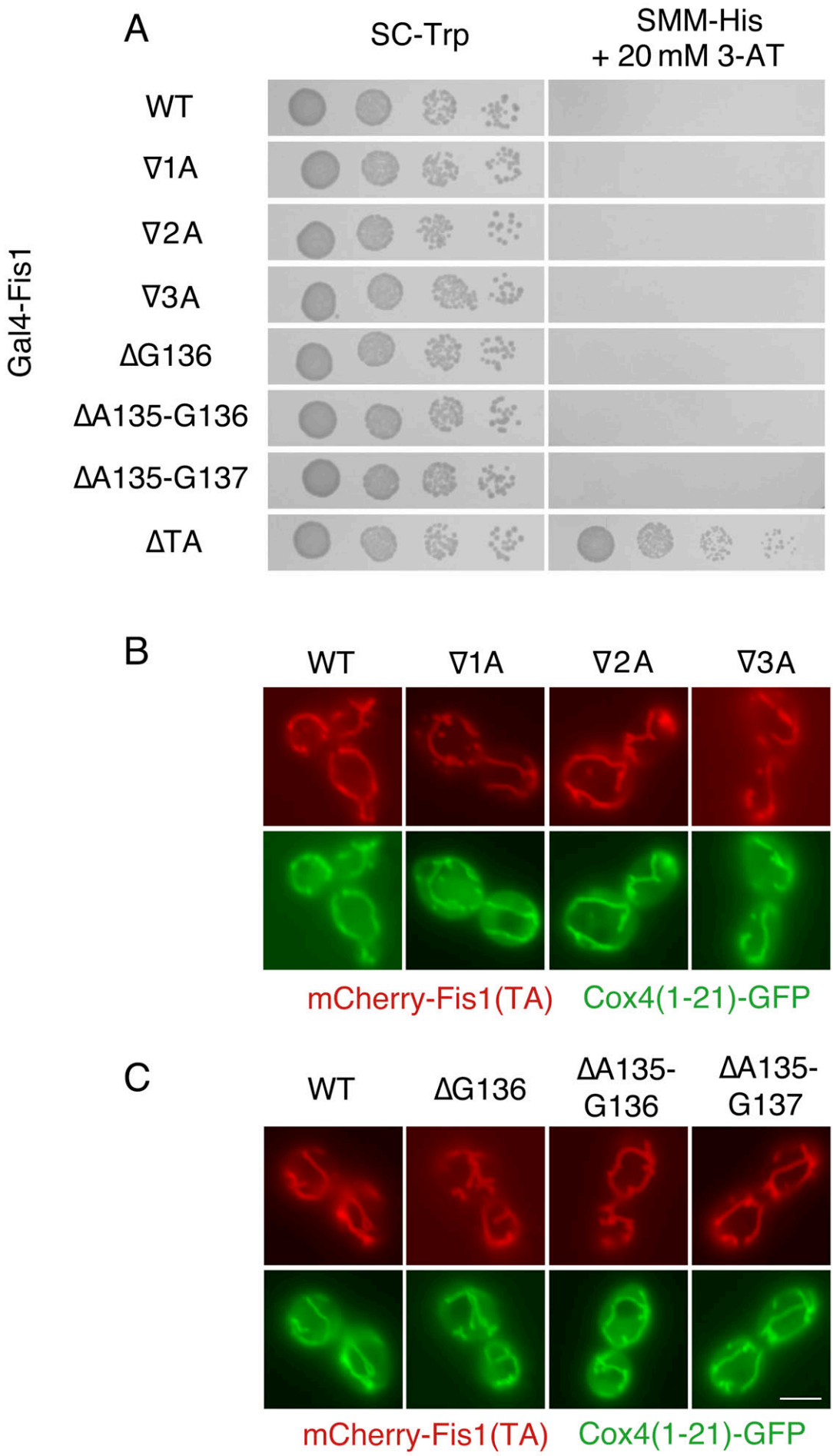
A
SC-Trp
SMM-His
+ 20 mM 3-AT
Gal4-Fis1
WT
∇1A
∇2A
∇3A
ΔG136
ΔA135-G136
ΔA135-G137
ΔTA
B
WT
∇1A
∇2A
∇3A
mCherry-Fis1(TA)
Cox4(1-21)-GFP
C
WT
ΔG136
ΔA135-
G136
ΔA135-
G137
mCherry-Fis1(TA)
Cox4(1-21)-GFP

Figure 6

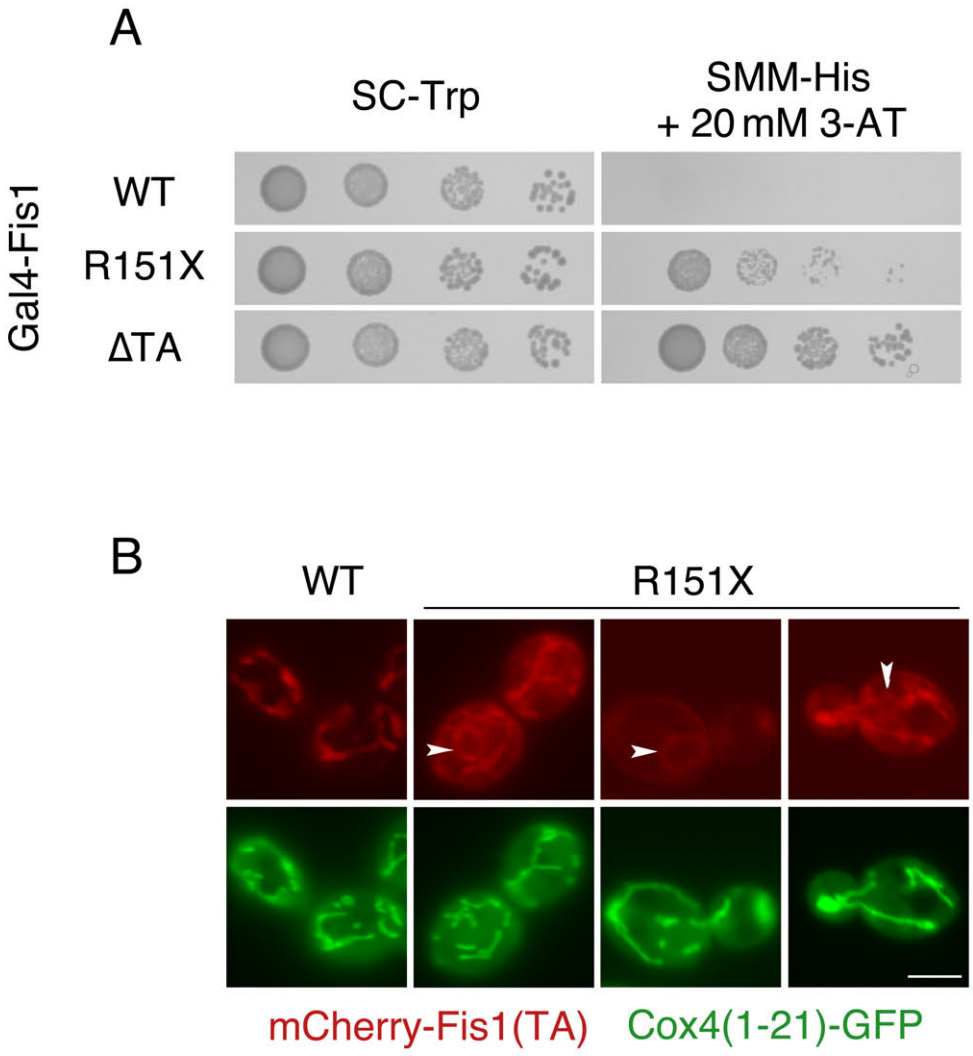
A
SC-Trp
SMM-His
+ 20 mM 3-AT
Gal4-Fis1
WT
R151X
ΔTA
B
WT
R151X
mCherry-Fis1(TA)
Cox4(1-21)-GFP

Figure 7

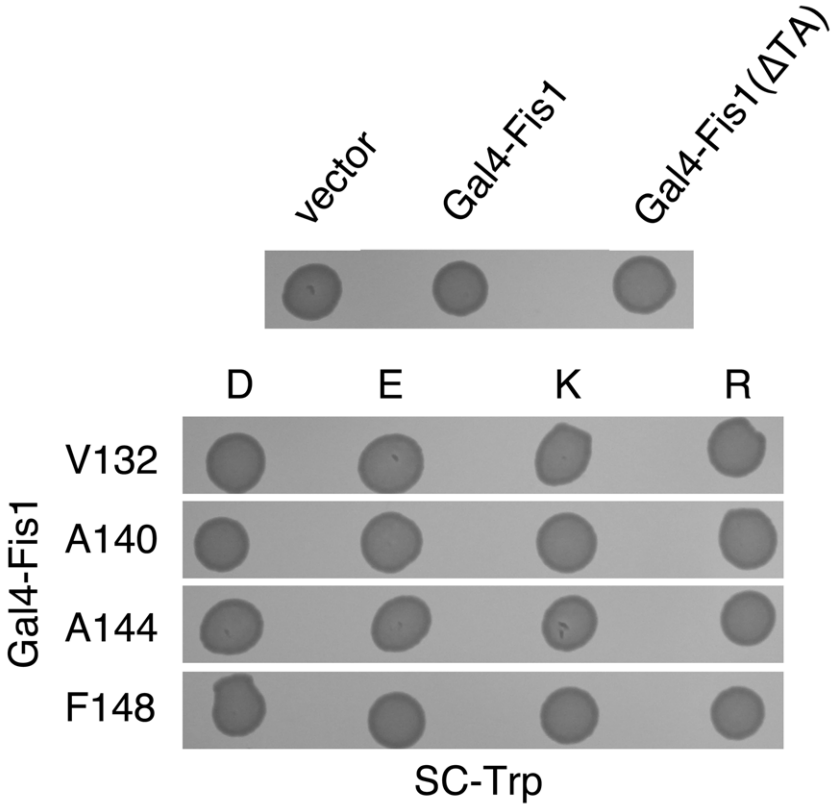
vector
Gal4-Fis1
Gal4-Fis1(ΔTA)
D
E
K
R
V132
A140
A144
F148
Gal4-Fis1
SC-Trp

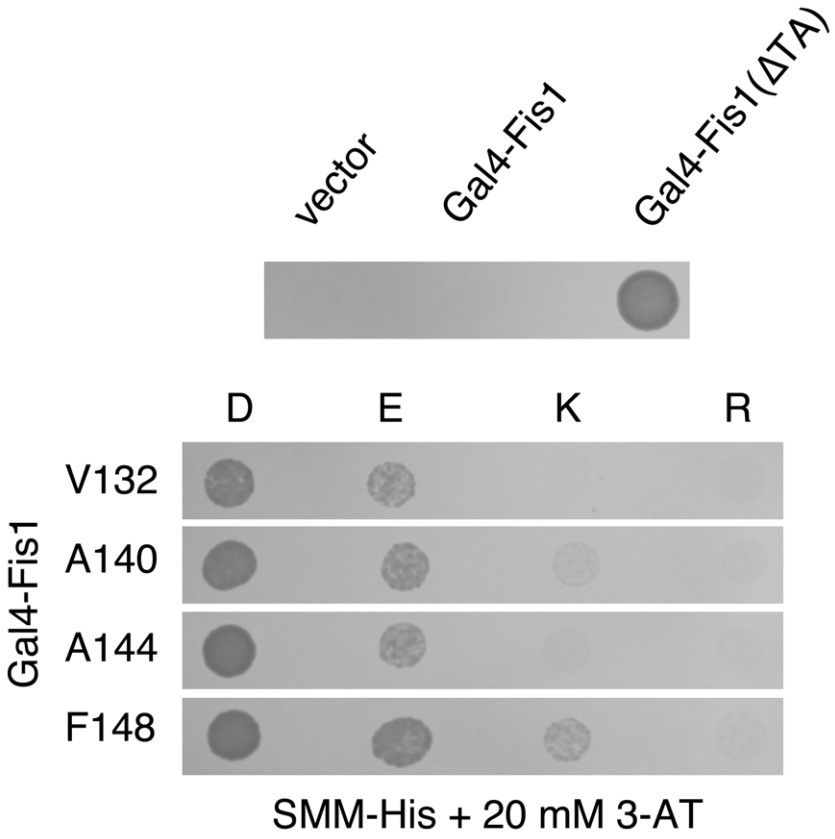
vector
Gal4-Fis1
Gal4-Fis1(ΔTA)
D
E
K
R
V132
A140
A144
F148
Gal4-Fis1
SMM-His + 20 mM 3-AT

Figure 8

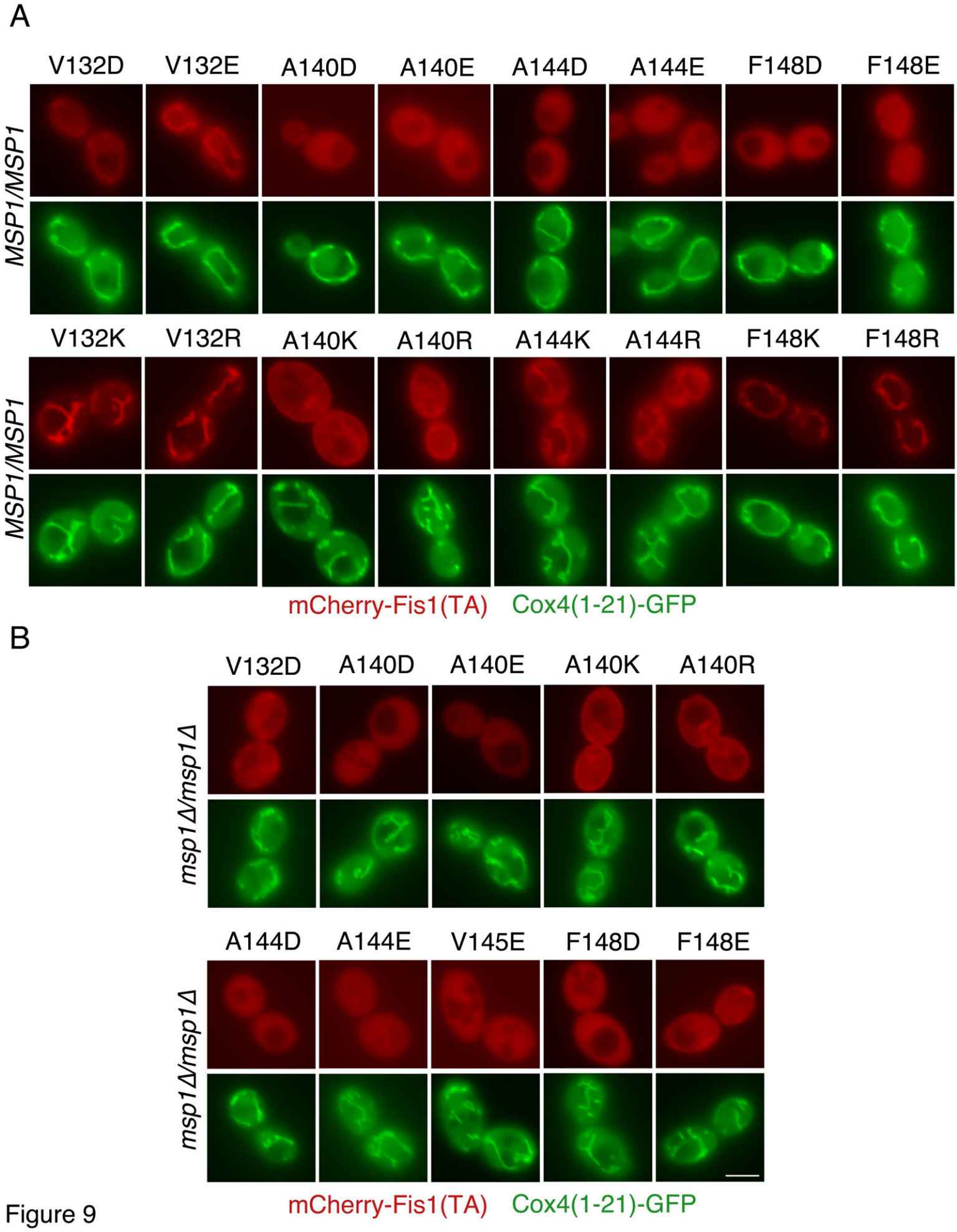
A
V132D
V132E
A140D
A140E
A144D
A144E
F148D
F148E
MSP1/MSP1
V132K
V132R
A140K
A140R
A144K
A144R
F148K
F148R
MSP1/MSP1
mCherry-Fis1(TA)
Cox4(1-21)-GFP
B
V132D
A140D
A140E
A140K
A140R
msp1Δ/msp1Δ
A144D
A144E
V145E
F148D
F148E
msp1Δ/msp1Δ
mCherry-Fis1(TA)
Cox4(1-21)-GFP

Figure 9

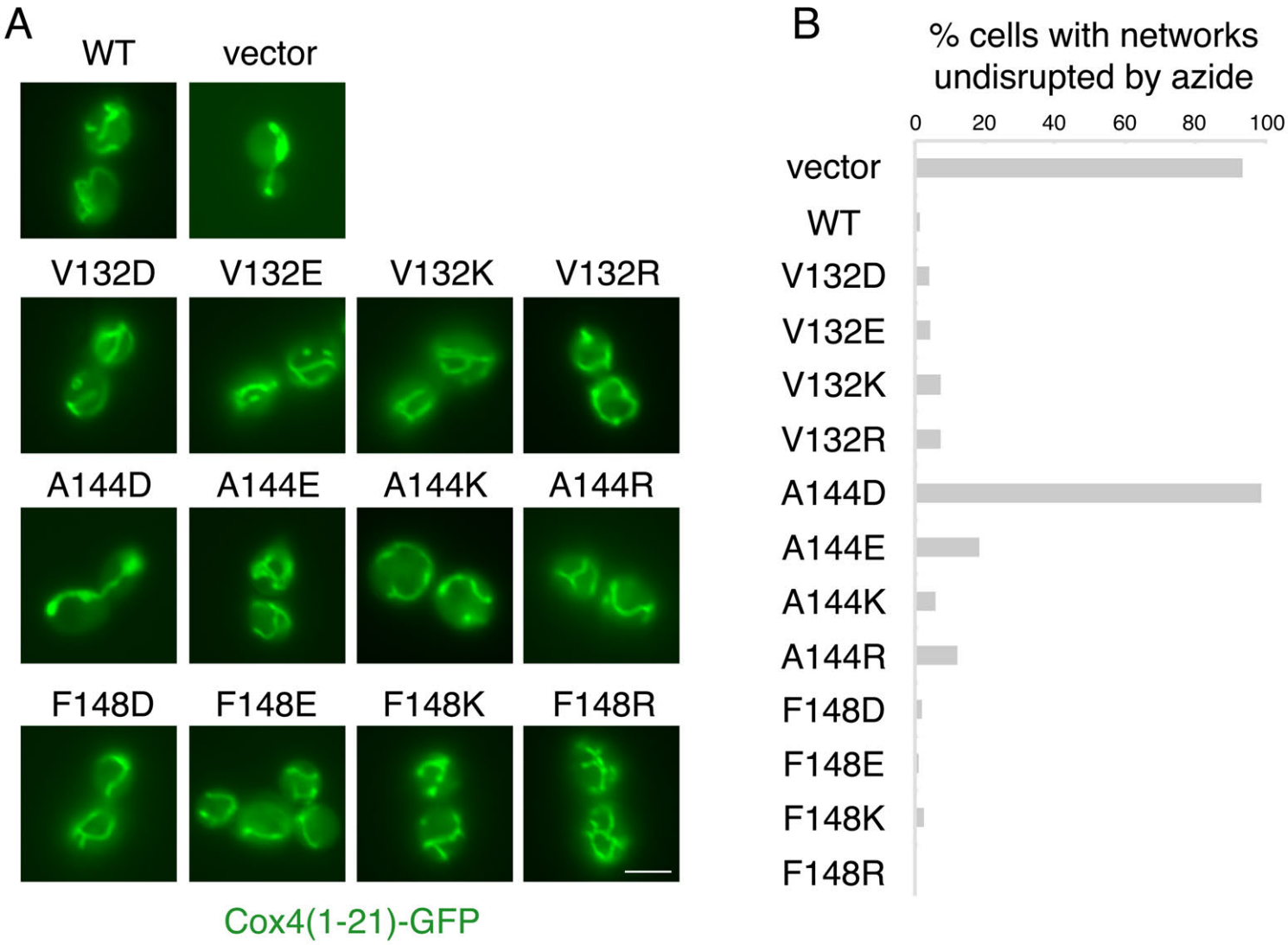
A
WT
vector
V132D
V132E
V132K
V132R
A144D
A144E
A144K
A144R
F148D
F148E
F148K
F148R
Cox4(1-21)-GFP
B
% cells with networks undisrupted by azide
0
20
40
60
80
100
vector
WT
V132D
V132E
V132K
V132R
A144D
A144E
A144K
A144R
F148D
F148E
F148K
F148R

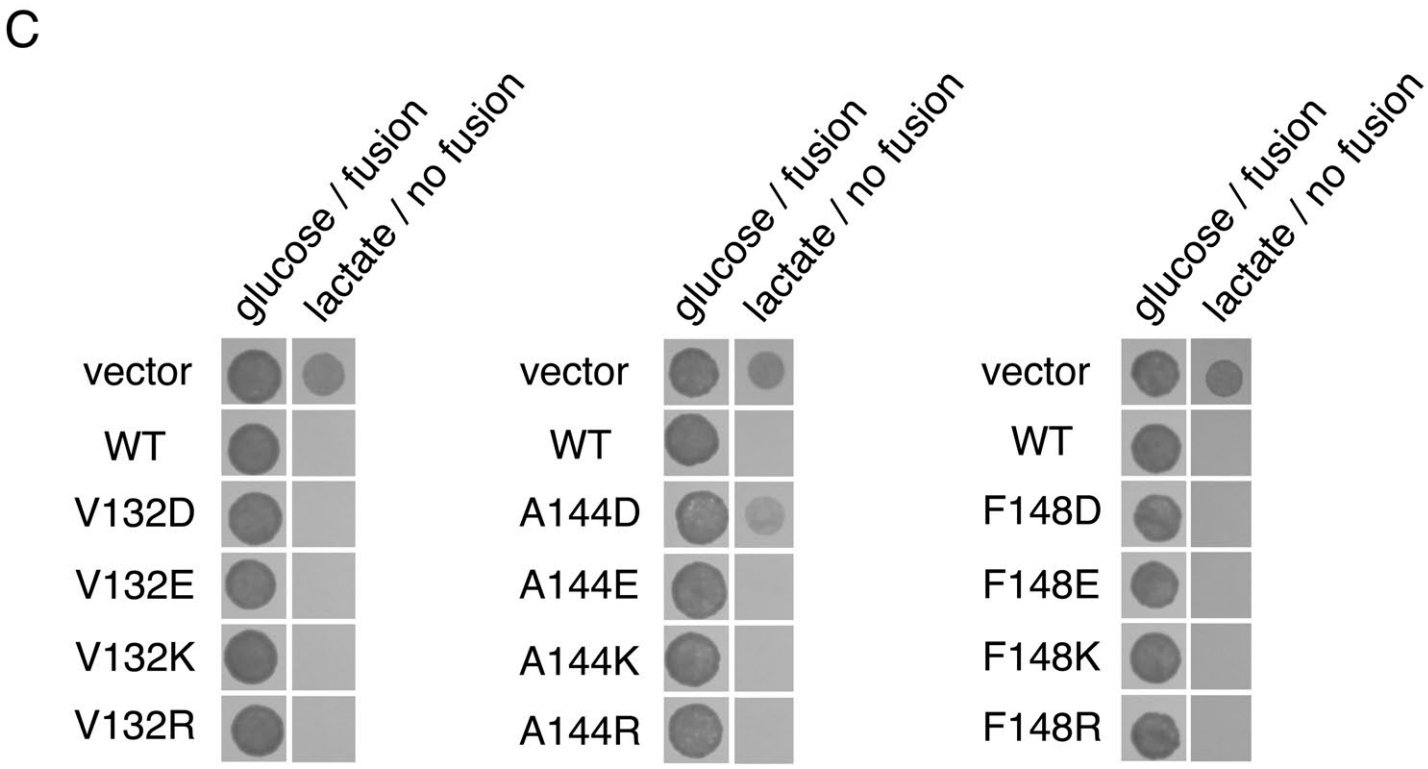
C
glucose / fusion
lactate / no fusion
vector
WT
V132D
V132E
V132K
V132R
glucose / fusion
lactate / no fusion
vector
WT
A144D
A144E
A144K
A144R
glucose / fusion
lactate / no fusion
vector
WT
F148D
F148E
F148K
F148R

Figure 10

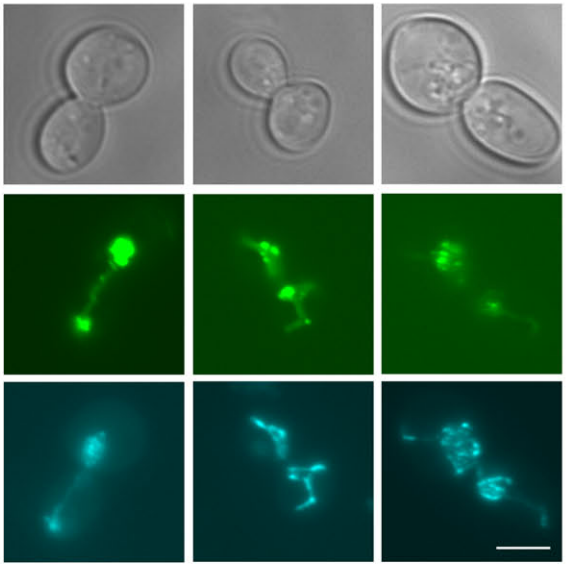

Figure S1

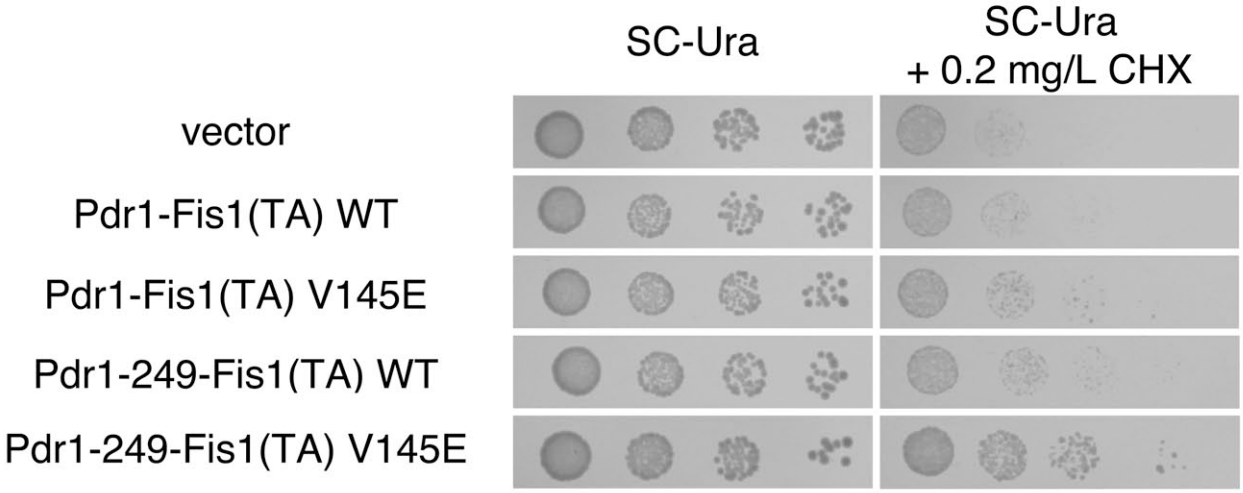
SC-Ura
SC-Ura
+ 0.2 mg/L CHX
vector
Pdr1-Fis1(TA) WT
Pdr1-Fis1(TA) V145E
Pdr1-249-Fis1(TA) WT
Pdr1-249-Fis1(TA) V145E

Figure S2

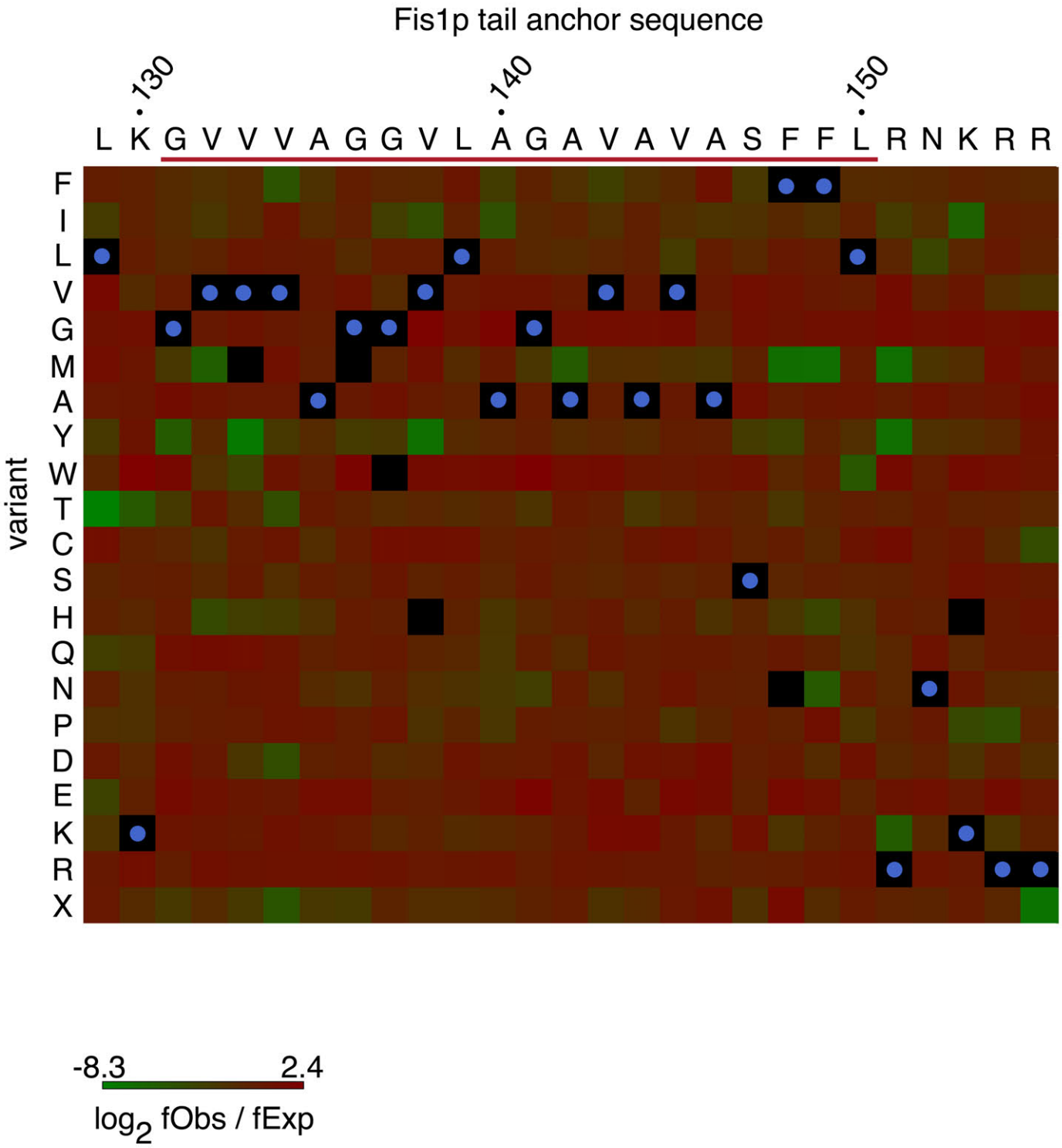
Fis1p tail anchor sequence
130
140
150
L K G V V V A G G V L A G A V A V A S F F L R N K R R
variant
F
I
L
V
G
M
A
Y
W
T
C
S
H
Q
N
P
D
E
K
R
X
-8.3
2.4
log2 fObs / fExp

Figure S3

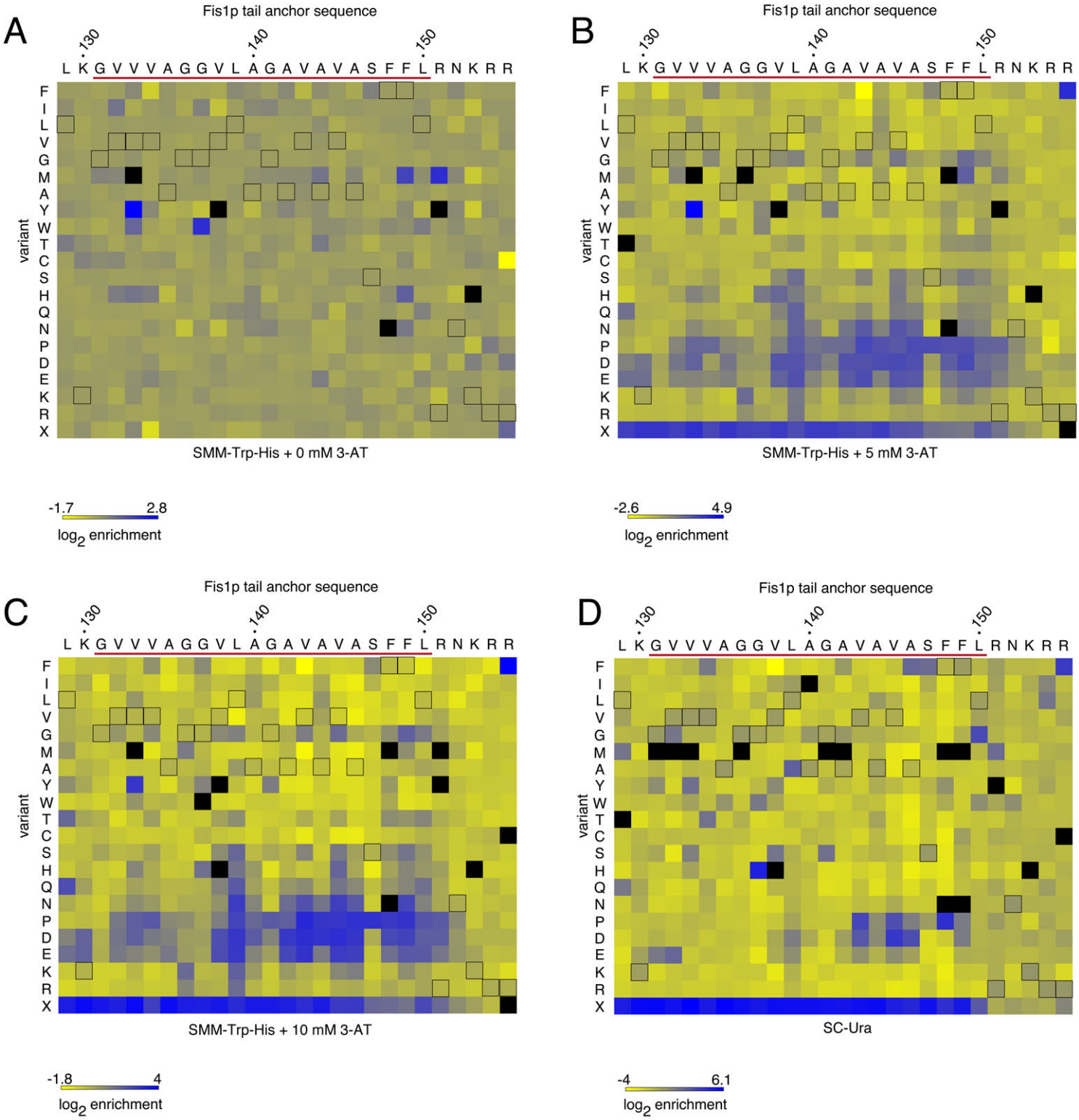
A
Fis1p tail anchor sequence
130
140
150
L K G V V V A G G V L A G A V A V A S F F L R N K R R
variant
F I L V G M A Y W T C S H Q N P D E K R X
SMM-Trp-His + 0 mM 3-AT
-1.7
2.8
log2 enrichment
B
Fis1p tail anchor sequence
130
140
150
L K G V V V A G G V L A G A V A V A S F F L R N K R R
variant
F I L V G M A Y W T C S H Q N P D E K R X
SMM-Trp-His + 5 mM 3-AT
-2.6
4.9
log2 enrichment
C
Fis1p tail anchor sequence
130
140
150
L K G V V V A G G V L A G A V A V A S F F L R N K R R
variant
F I L V G M A Y W T C S H Q N P D E K R X
SMM-Trp-His + 10 mM 3-AT
-1.8
4
log2 enrichment
D
Fis1p tail anchor sequence
130
140
150
L K G V V V A G G V L A G A V A V A S F F L R N K R R
variant
F I L V G M A Y W T C S H Q N P D E K R X
SC-Ura
-4
6.1
log2 enrichment

Figure S4

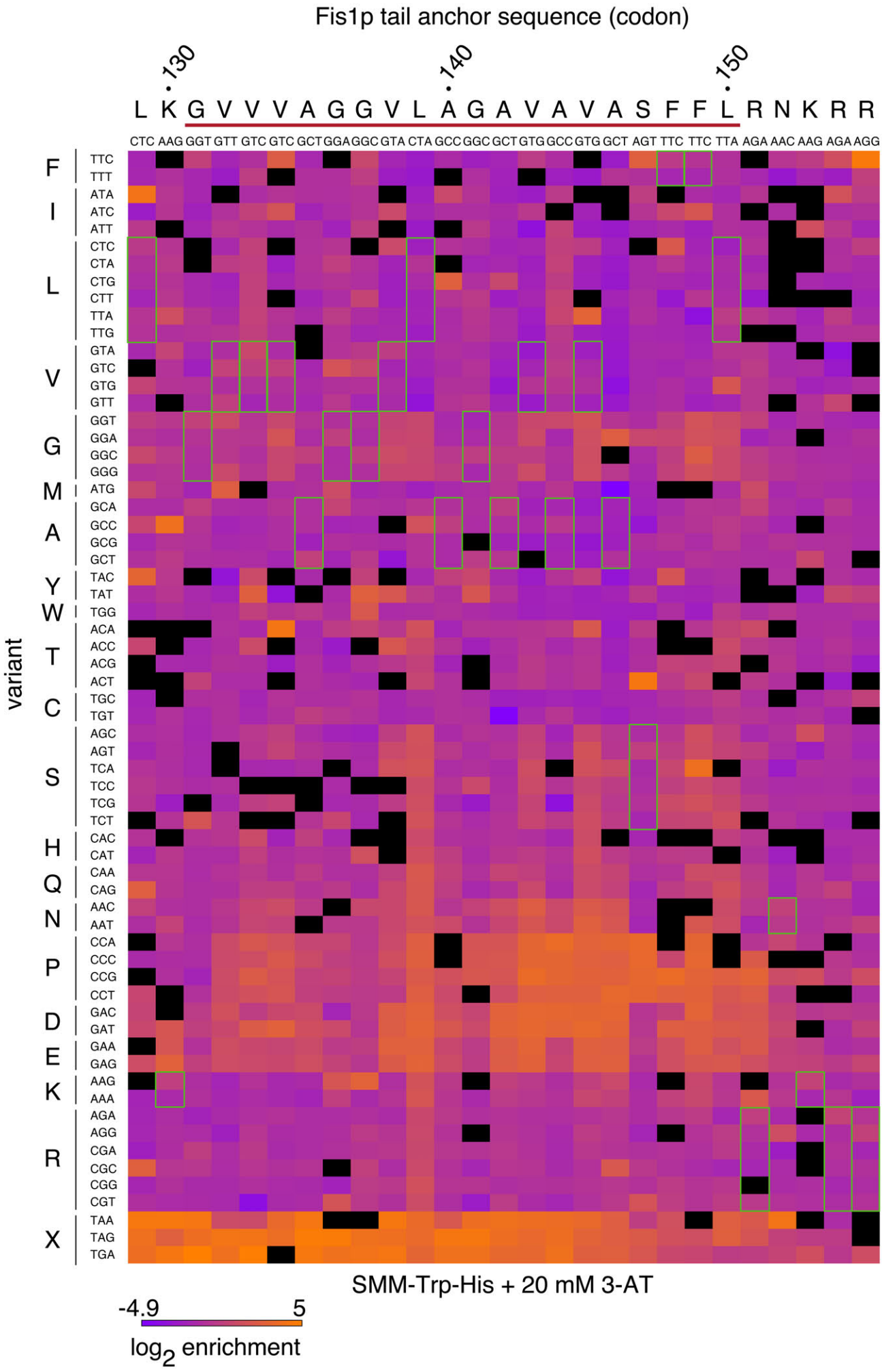
Fis1p tail anchor sequence (codon)
130
140
150
L K G V V V A G G V L A G A V A V A S F F L R N K R R
CTC AAG GGT GTT GTC GTC GCT GGA GGC GTA CTA GCC GGC GCT GTG GCC GTG GCT AGT TTC TTC TTA AGA AAC AAG AGA AGG
variant
F TTC TTT
I ATA ATC ATT
L CTC CTA CTG CTT TTA TTG
V GTA GTC GTG GTT
G GGT GGA GGC GGG
M ATG
A GCA GCC GCG GCT
Y TAC TAT
W TGG
T ACA ACC ACG ACT
C TGC TGT
S AGC AGT TCA TCC TCG TCT
H CAC CAT
Q CAA CAG
N AAC AAT
P CCA CCC CCG CCT
D GAC GAT
E GAA GAG
K AAG AAA
R AGA AGG CGA CGC CGG CGT
X TAA TAG TGA
SMM-Trp-His + 20 mM 3-AT
-4.9
5
log2 enrichment

Figure S5

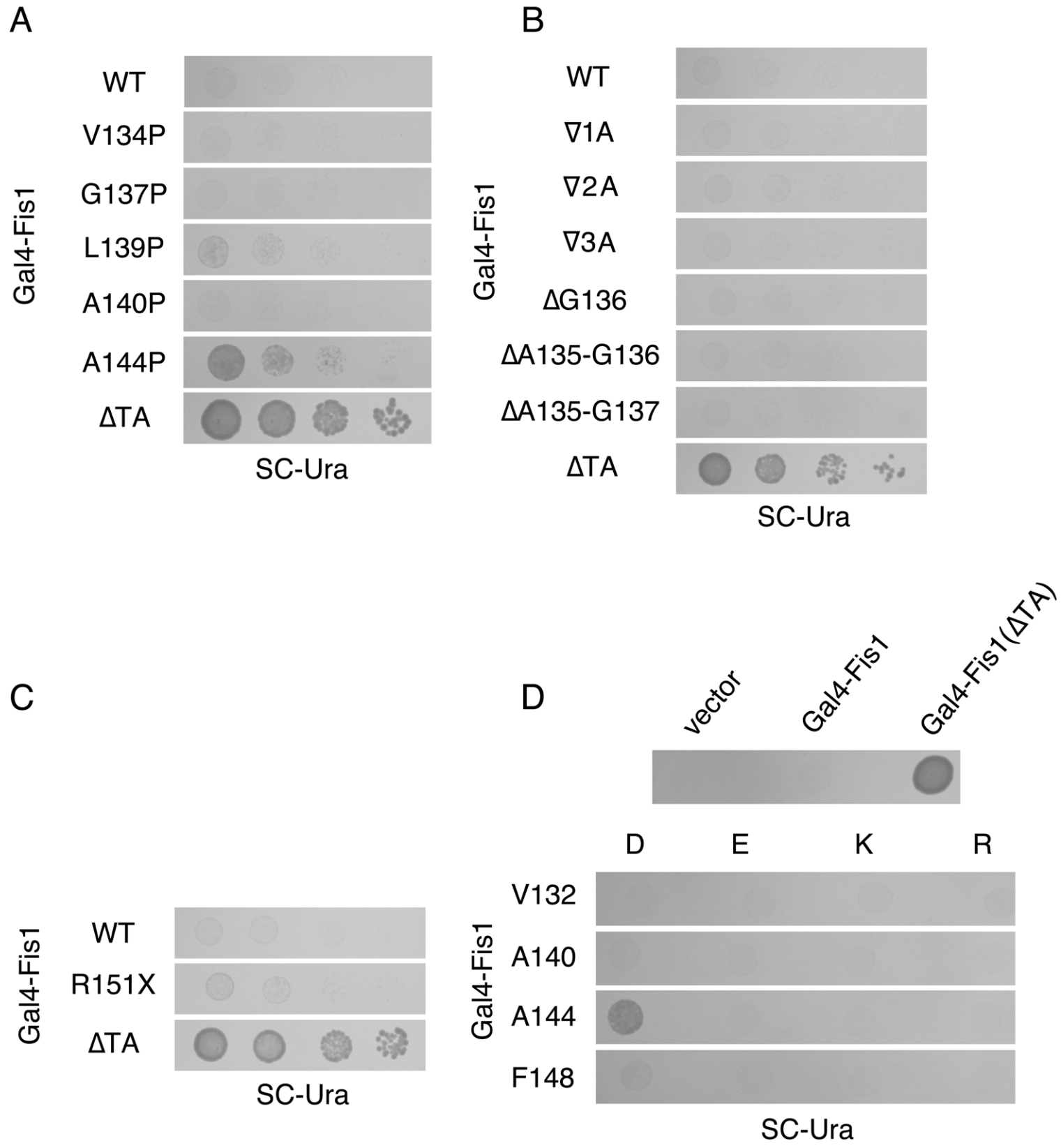
A
Gal4-Fis1
WT
V134P
G137P
L139P
A140P
A144P
ΔTA
SC-Ura
B
Gal4-Fis1
WT
∇1A
∇2A
∇3A
ΔG136
ΔA135-G136
ΔA135-G137
ΔTA
SC-Ura
C
Gal4-Fis1
WT
R151X
ΔTA
SC-Ura
D
vector
Gal4-Fis1
Gal4-Fis1(ΔTA)
D
E
K
R
Gal4-Fis1
V132
A140
A144
F148
SC-Ura

Figure S6

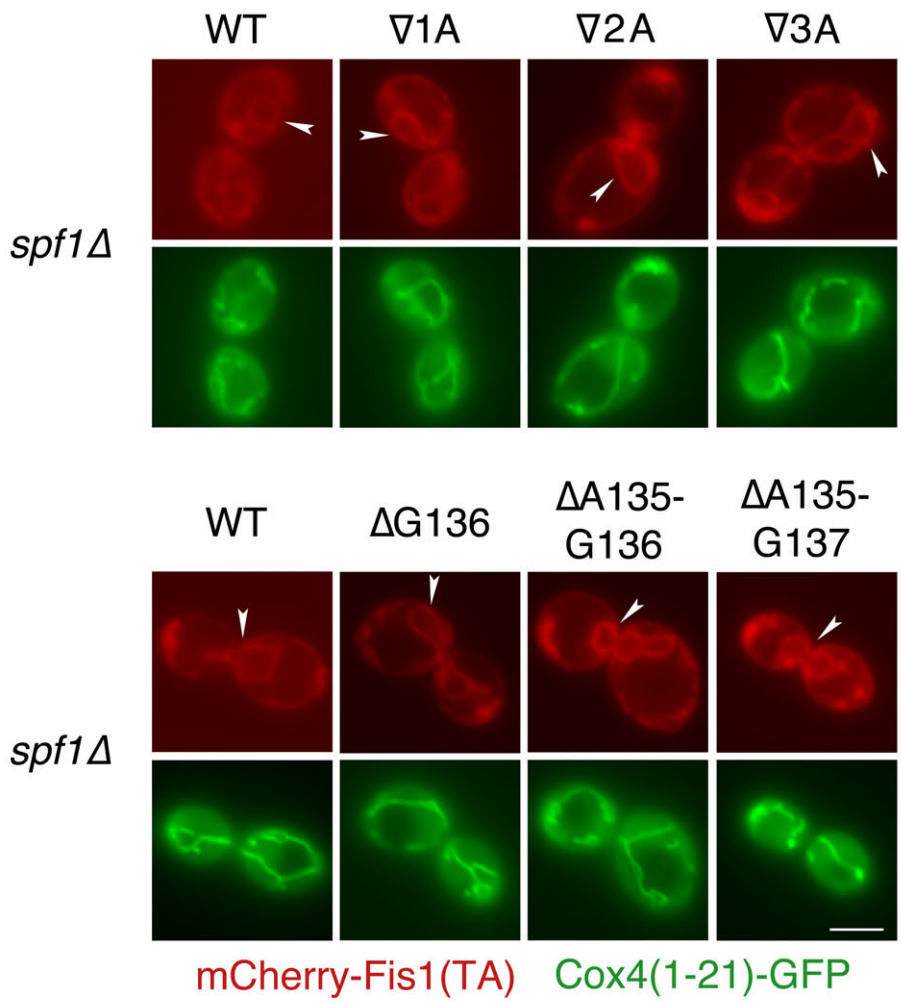
WT
∇1A
∇2A
∇3A
spf1Δ
WT
ΔG136
ΔA135-G136
ΔA135-G137
spf1Δ
mCherry-Fis1(TA)
Cox4(1-21)-GFP

Figure S7

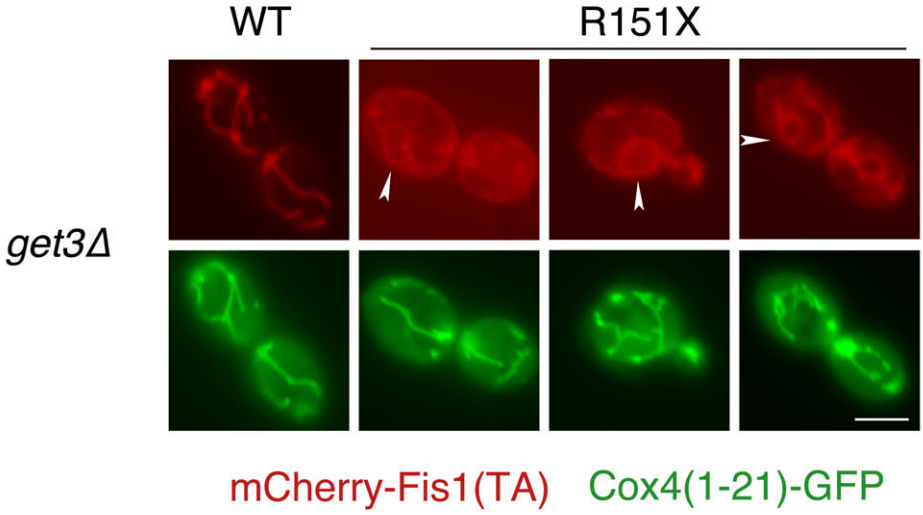

Figure S8

A

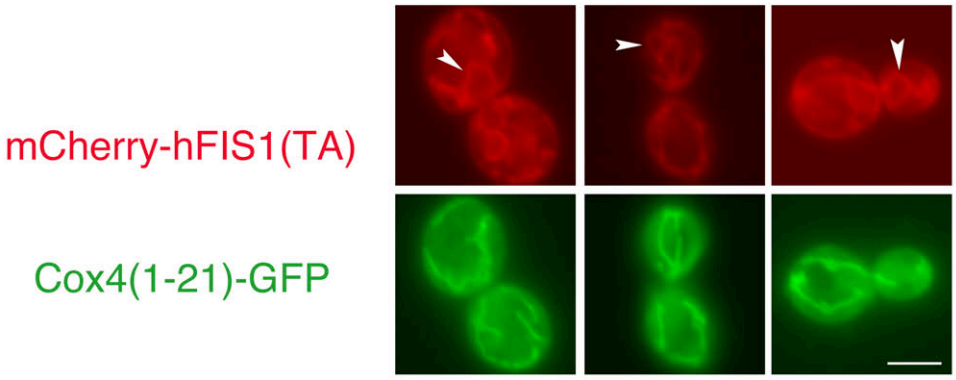

B

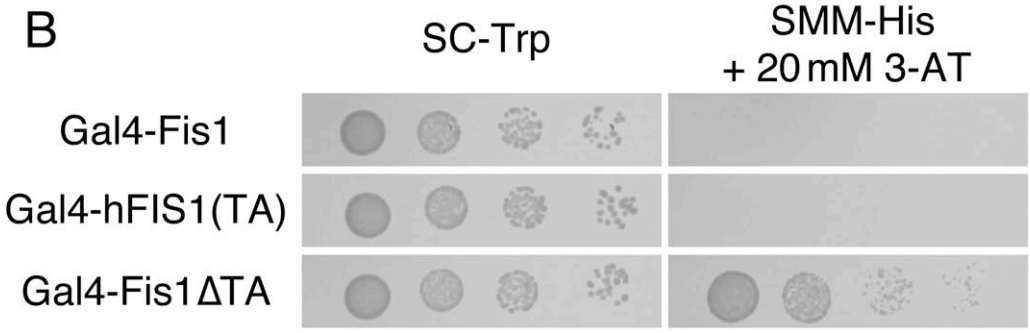

C

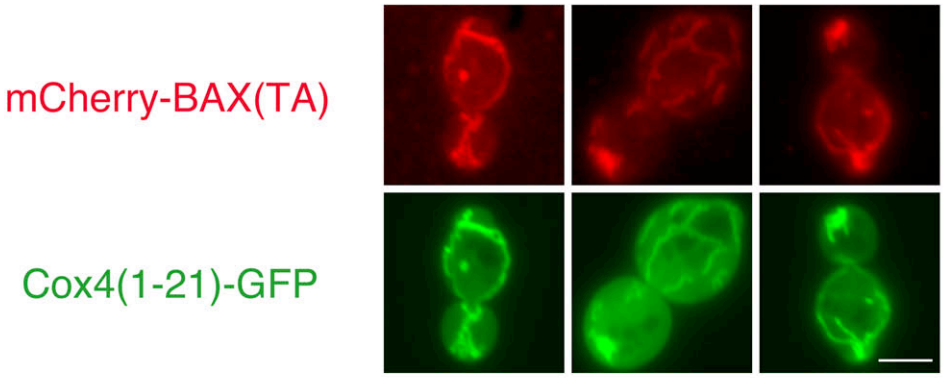

Figure S9

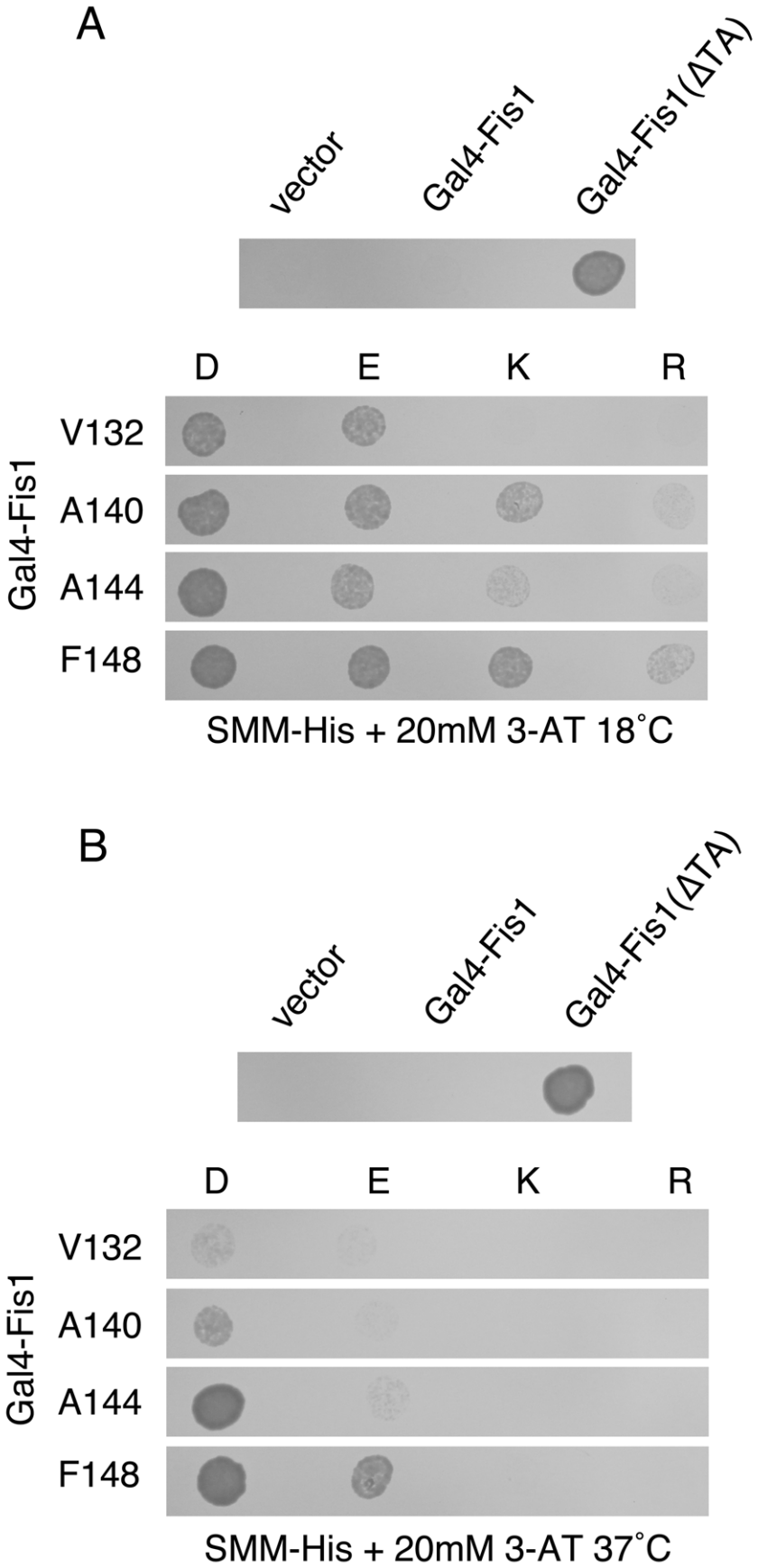
A
vector
Gal4-Fis1
Gal4-Fis1(ΔTA)
D
E
K
R
Gal4-Fis1
V132
A140
A144
F148
SMM-His + 20mM 3-AT 18˚C
B
vector
Gal4-Fis1
Gal4-Fis1(ΔTA)
D
E
K
R
Gal4-Fis1
V132
A140
A144
F148
SMM-His + 20mM 3-AT 37˚C

Figure S10

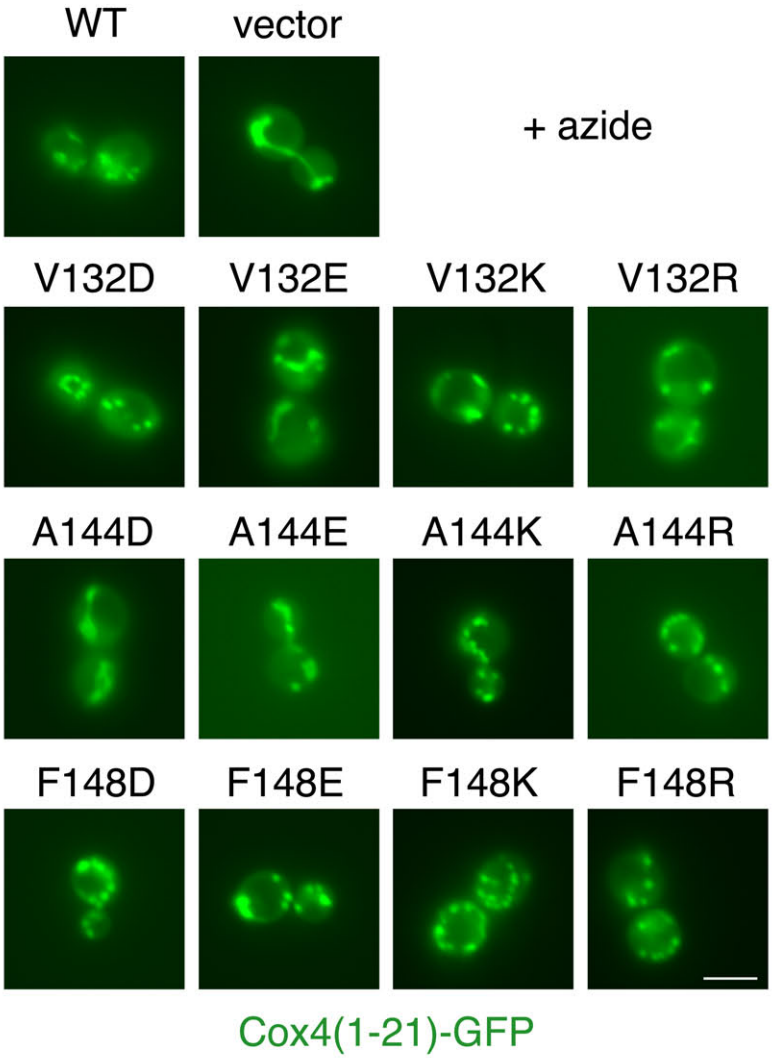
WT
vector
+ azide
V132D
V132E
V132K
V132R
A144D
A144E
A144K
A144R
F148D
F148E
F148K
F148R
Cox4(1-21)-GFP

Figure S11